AD-A117 286 SCIENCE APPLICATIONS INC MCLEAN VA F/G 8/3
STATISTICAL ANALYSIS OF UPPER OCEAN TIME SERIES OF VERTICAL SHE--ETC(U)
MAY 82 D M RUBENSTEIN, F C NEWMAN N00014-81-C-0075
UNCLASSIFIED SAI-83-751-WA NL

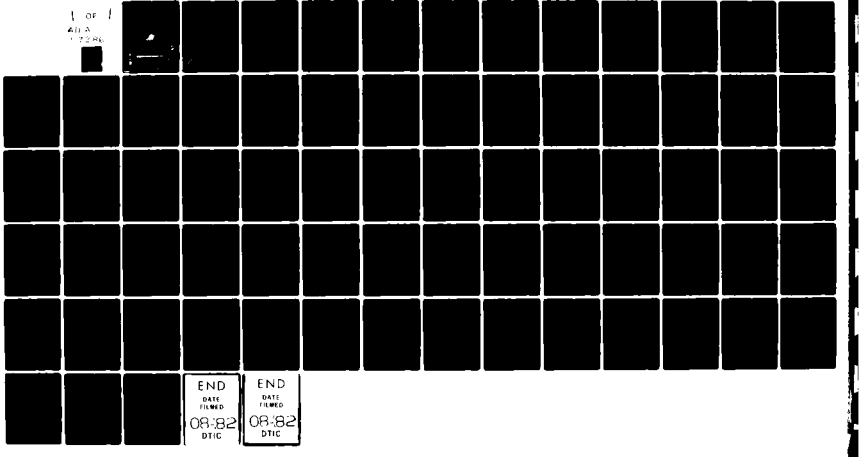

END DATE FILMED 08-82 DTIC

END DATE FILMED 08-82 DTIC

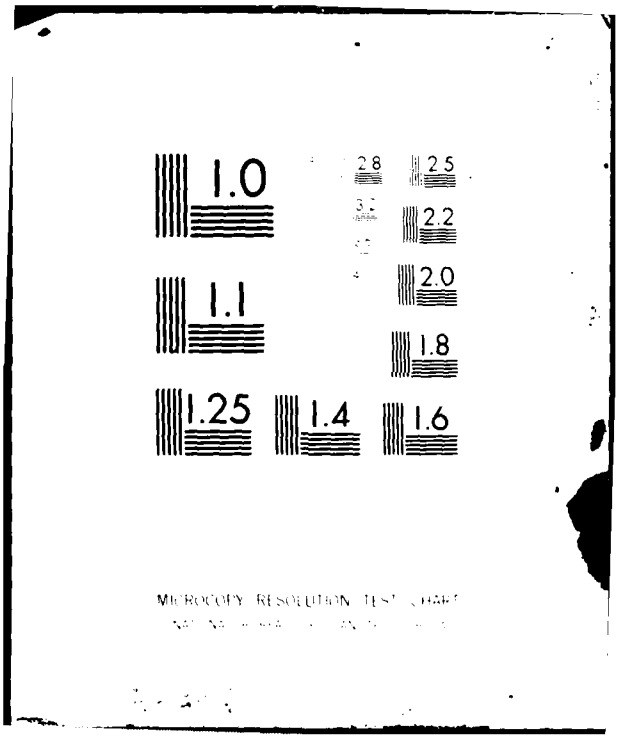
1.0
2.8
2.5
2.2
2.0
1.1
1.8
1.25
1.4
1.6
MICROCOPY RESOLUTION TEST CHART

(12)

# STATISTICAL ANALYSIS OF UPPER OCEAN TIME SERIES OF VERTICAL SHEAR

SAI-83-751-WA

A



SAI

ATLANTA • ANN ARBOR • BOSTON • CHICAGO • CLEVELAND • DENVER • HUNTSVILLE • LA JOLLA
LITTLE ROCK • LOS ANGELES • SAN FRANCISCO • SANTA BARBARA • TUCSON • WASHINGTON

# STATISTICAL ANALYSIS OF UPPER OCEAN TIME SERIES OF VERTICAL SHEAR

SAI-83-751-WA

OPD-TR-82-257-01

May 1982

Prepared by:

David M. Rubenstein
Fred C. Newman

Prepared for:

Naval Ocean Research and Development Activity
Ocean Measurements Program, Code 540
NSTL Station, Mississippi 39529

Final Report for Contract No. N00014-81-C-0075

SCIENCE APPLICATIONS, INC.

1710 Goodridge Drive
P.O. Box 1303
McLean, Virginia 22102
(703) 821-4300

UNCLASSIFIED

SECURITY CLASSIFICATION OF THIS PAGE (When Data Entered)

| REPORT DOCUMENTATION PAGE | READ INSTRUCTIONS BEFORE COMPLETING FORM |
|---|---|
| 1 REPORT NUMBER: SAI-83-751-WA | 2 GOVT ACCESSION NO: AD-A117286 | 3 RECIPIENT'S CATALOG NUMBER: |
| 4 TITLE and Subtitle: Statistical Analysis of Upper Ocean Time Series of Vertical Shear | 5 TYPE OF REPORT & PERIOD COVERED: Final Report 10/81 - 4/82 |
| | 6 PERFORMING ORG. REPORT NUMBER: SAI-83-751-WA |
| 7 AUTHOR(s): David M. Rubenstein, Fred C. Newman | 8 CONTRACT OR GRANT NUMBER(s): N00014-81-C-0075 |
| 9 PERFORMING ORGANIZATION NAME AND ADDRESS: Science Applications, Inc. 1710 Goodridge Drive, P.O. Box 1303 McLean, Virginia 22102 | 10 PROGRAM ELEMENT, PROJECT, TASK AREA & WORK UNIT NUMBERS |
| 11 CONTROLLING OFFICE NAME AND ADDRESS: NORDA Code 540 Ocean Measurements Program NSTL Station, Bay St. Louis, MS 39529 | 12 REPORT DATE: May 1982 |
| | 13 NUMBER OF PAGES: 65 |
| 14 MONITORING AGENCY NAME & ADDRESS(if different from Controlling Office) | 15 SECURITY CLASS. (of this report): UNCLASSIFIED |
| | 15a DECLASSIFICATION DOWNGRADING SCHEDULE |

16 DISTRIBUTION STATEMENT (of this Report)

Approved for public release; distribution unlimited

17 DISTRIBUTION STATEMENT (of the abstract entered in Block 20, if different from Report)

Approved for public release; distribution unlimited

18 SUPPLEMENTARY NOTES

19 KEY WORDS (Continue on reverse side if necessary and identify by block number)

Vertical Shear
Shear
Inertial Oscillations
Statistical Modeling
Current Meter
VACM
Upper Ocean Shear

20 ABSTRACT (Continue on reverse side if necessary and identify by block number)

Shear measurements from the MILE current meter observations are statistically analyzed. Much of the shear is inertial, and probability density histograms of short-term records are bimodal. Over three inertial periods, shear distribution approaches Gaussianity.

We derive a simple statistical model of shear, which predicts how mean-square shear varies with stratification and vertical separation $\Delta z$. We compare these predictions with MILE observations.

DD FORM 1 JAN 73 1473 EDITION OF 1 NOV 65 IS OBSOLETE

UNCLASSIFIED

SECURITY CLASSIFICATION OF THIS PAGE (When Data Entered)

We also show that 15-minute average samples of $N^2$ and $S^2$ are significantly correlated. Knowing the 15-minute average value of $N^2$ allows one to predict $S^2$ within a factor of two at least 46% of the time, and within a factor of four at least 75% of the time.



A

TABLE OF CONTENTS


| Section | | Page |
|---|---|---|
| 1 | INTRODUCTION AND BACKGROUND | 1-1 |
| 2 | DATA PROCESSING | 2-1 |
| | 2.1 Current Meters and Filtering | 2-1 |
| | 2.2 Density Stratification from Temperature Gradients | 2-3 |
| 3 | TEMPORAL VARIABILITY OF SHEAR DISTRIBUTION | 3-1 |
| | 3.1 Complex Demodulation | 3-1 |
| | 3.2 Distribution of Inertial Oscillations | 3-6 |
| | 3.3 Long-Term Gaussian Distribution | 3-9 |
| 4 | STATISTICAL MODEL OF MEAN-SQUARE SHEAR | 4-1 |
| | 4.1 Predictions of Mean-Square Shear | 4-1 |
| | 4.2 Statistical Model-Data Comparisons | 4-5 |
| 5 | PROBABILITY DISTRIBUTION OF SHEAR | 5-1 |
| | 5.1 Preliminary Statistical Tests | 5-1 |
| | 5.1.1 Autocorrelation and Run Test for Randomness | 5-1 |
| | 5.1.2 Smirnov Test for Identical Distributions | 5-5 |
| | 5.2 Lilliefors Test for Gaussianity | 5-6 |
| | 5.3 Statistical Model Application: The Kolmogorov Test | 5-11 |
| 6 | INSTANTANEOUS PREDICTIONS OF SHEAR | 6-1 |
| 7 | SUMMARY AND RECOMMENDATIONS | 7-1 |
| | REFERENCES | R-1 |

LIST OF FIGURES


| Figure | | Page |
|---|---|---|
| 2.1 | Profiles of temperature and salinity | 2-4 |
| 2.2 | T-S relation from CTD casts | 2-4 |
| 3.1 | Rotary spectra of velocity difference | 3-2, 3-3 |
| 3.2 | Complex demodulation of velocity difference | 3-5 |
| 3.3 | Probability density functions for inertial oscillations | 3-8 |
| 3.4 | Vector trace of velocity difference | 3-10 |
| 3.5 | Shear distribution over an inertial period | 3-11 |
| 3.6 | Skewness, kurtosis-3, and Lilliefors test statistic for Gaussianity, for 48-hr records of shear over depth interval 47-50 m | 3-13 |
| 4.1 | Idealized shear spectrum | 4-3 |
| 4.2 | $\overline{S^2}$ vs. $\overline{N^2}$ from eight pairs of current meters with $\Delta z$ = 3 m | 4-7 |
| 4.3 | $\overline{S^2}$ vs. $\overline{N^2}$ from seven pairs of current meters with $\Delta z$ = 6 m | 4-8 |
| 4.4 | $\overline{S^2}$ vs. $\overline{N^2}$ from five pairs of current meters with $\Delta z$ = 12 m | 4-9 |
| 4.5 | $\overline{S^2}$ vs. $\overline{N^2}$ from three pairs of current meters with $\Delta z$ = 21 m | 4-10 |
| 4.6 | Comparison between observed and modeled mean-square velocity difference | 4-12 |
| 5.1 | Autocorrelation of shear over depth interval 29-32 m | 5-3 |
| 5.2 | Autocorrelation of shear over depth interval 41-44 m | 5-4 |
| 5.3 | Probability density histogram of shear over 41-44 m, for 19-day record | 5-8 |
| 5.4 | Cumulative distribution of shear over 41-44 m, for 19-day record | 5-10 |

LIST OF FIGURES (continued)


| Figure | | Page |
|---|---|---|
| 6.1 | Time series of 15-minute averaged samples of $N^2$ and $S^2$, over 29-32 m | 6-2 |
| 6.2 | Probability density histogram of $S^2/N^2$ over 41-44 m | 6-5 |
| 6.3 | Cumulative distribution function of $S^2/N^2$ over 41-44 m | 6-6 |

LIST OF TABLES


| Table | | Page |
|---|---|---|
| 4.1 | Mean-square velocity differences | 4-5 |
| 4.2 | Least-squares regression coefficients $\overline{S^2} = b\overline{N^2}$ | 4-6 |
| 5.1 | Lilliefors Gaussianity test results | 5-11 |
| 5.2 | Kolmogorov goodness-of-fit test results | 5-13 |
| 6.1 | Lower and upper limits of linear correlation coefficients between 15-minute averaged observations of $N^2$ and $S^2$ | 6-4 |
| 6.2 | Average percentage of 15-minute $N^2$ observations from which we can predict $S^2$ within a factor of 2 and 4 | 6-7 |

# Section 1
# INTRODUCTION AND BACKGROUND

Vertical shear is the vertical gradient of horizontal velocity, and is important from several points of view. Details of the Navy interest in shear were summarized in an SAI report to NORDA (Lambert and Patterson; 1980), which reviewed the status of measurements of vertical shear in the upper ocean as of early 1980. The results of that report led us to focus our attention on describing and modeling shear over the scale range between 1 meter and a few tens of meters.

Navy applications include the potential effects of shear on subsurface wakes. Shear can kinematically distort a passive wake contaminant, and can interact with active wake signature fields, such as turbulence and internal waves. The oceanographic community is generally interested in fine-scale shear distribution because of the (still controversial) importance of shear instability in turbulence and mixing. The first approaches evaluated the contribution of internal wave motions to the shear field (Grabowski; 1980), and these focused first on vertical profiles and distributions in terms of vertical wavenumbers. These studies led to the confirmation of earlier studies, that the variability in the shear field is concentrated in the high-wavenumber end of the spectrum and in the low frequency (near-inertial) portion of the internal wave band.

A number of other studies have focused on statistical descriptions of the probability distribution of internal waves, concentrating on velocity or temperature fluctuations, but not specifically on shear. Briscoe (1977)

compiled the results of eight such studies. He noted that the most impressive result of his compilation is that contradictory results seem to emerge from similar experiments. Comparisons among evaluations of the Gaussianity of temperature fluctuations and currents yield no clear consensus. Briscoe suggested that this may indicate intermittency in the structure of the probability distribution. He examined the time variability of horizontal current, temperature, and vertical displacement data from the Internal Wave Experiment (IWEX). In the case of horizontal currents, he found that interludes of non-Gaussian statistics are related to kurtosis values of less than 3.

To the authors' knowledge, only two studies of shear statistics have been previously performed, both using data from free fall vertical profilers. Again, the results were contradictory. Simpson's (1975) observations of shear probability density functions over a length scale of about 35 cm were highly intermittent and non-Gaussian. Hebenstreit and Grabowski (1981) found that shear probability density functions over 2, 4, 8, and 16 m were almost all nearly Gaussian.

Vertical profiles of shear show a high degree of correlation between shear squared ($S^2$) and Vaisala frequency squared ($N^2$). Patterson et al. (1981) documented this correlation using profiles having vertical resolution between 2 m and 8 m. They also found that the correlation improves when $N^2$ and $S^2$ are low-pass filtered in the vertical. The implication is that $N^2$ and $S^2$ are better correlated over length scales in the range between 5 m and 20 m than over a 2 m length scale.

The majority of vertical shear observations have been made using vertical profiling instruments. Gargett et al. (1981) describe a composite vertical wavenumber spectrum of upper ocean shear from three different velocity profilers. Each of the instruments is effective over a limited range of vertical length scales, and by carefully comparing their spectra, Gargett et al. form a composite shear spectrum over vertical wavelengths ranging from a few centimeters up to more than 100 m. In the low wavenumber portion $0 < k \lesssim .1$ cpm, they find that the shear spectral density is approximately independent of wavenumber, and, as a consequence, scales according to $N^2$. This result is consistent with the previously-noted point-wise correlation between shear and stratification. The results are most reliable in the deeper thermocline where N does not vary rapidly with depth.

A similar correlation is observed in current meter time series--a quite different type of data set. Eriksen (1978) measured velocity differences over a fixed separation of 7 m in the main thermocline near Bermuda, and found that the shear was constrained such that the Richardson number $Ri = N^2/S^2$ was almost always greater than about 1/4. Davis et al. (1981) observed a very similar Richardson number constraint acting on 15-min averages of shear calculated over 3 m vertical spacing during MILE (Mixed Layer Experiment).

In the seasonal thermocline, $N^2$ varies rapidly with depth. Thus shear statistics derived from vertical profiler data in the seasonal thermocline are nonstationary in depth. Therefore, vertical wavenumber spectra of shear are probably not statistically reliable, especially in the low wavenumber band. But it is possible, using pairs of

current meters separated by a range of vertical separations $\Delta z$, to extract useful information about the vertical scales of shear in the seasonal thermocline. One of the chief objectives of this report is to evaluate a statistical model which is capable of relating the statistics of shear calculated from vertical profilers to the statistics of shear calculated from current meters. The model is derived from an idealized version of the Gargett et al. spectrum, and the data set used is the set of current meter records from MILE. The success of this model allows us to extend the range of validity of the composite spectrum of Gargett et al. (1981) into the seasonal thermocline.

This report is organized as follows. In Section 2 we discuss the MILE data set, including the current meter response, the contamination of current measurements due to mooring motions, and the low-pass filter used to remove unwanted noise. We also show how $N^2$ was computed from time series of $\Delta T/\Delta z$ combined with T-S relations calculated from averaged CTD profiles. In Section 3 we discuss the temporal variability of shear distribution, showing that shear is dominated by inertial oscillations.

In Section 4 we describe the development of the statistical model of mean-square shear based on an idealized version of the composite vertical shear spectrum. The model predicts mean square shear as a function of vertical separation $\Delta z$ and mean square Vaisala frequency, and is compared with shear observations from current meter time series. In Section 5 we use this model to show that shear distribution recorded over many inertial periods is reasonably Gaussian.

In Section 6 we consider the correlation between $N^2$ and $S^2$ over very short time scales (15-minute

averages). The correlation is shown to be significant, and we also show from the distribution functions of $S^2/N^2$, that knowing the value of $N^2$ allows one to predict $S^2$ within a factor of two at least 46% of the time, and within a factor of four at least 75% of the time.

In Section 7 we summarize the conclusions and recommend possible directions for future work.

# Section 2
# DATA PROCESSING

## 2.1 CURRENT METERS AND FILTERING

The current meter data from the MILE-1 mooring provide good vertical resolution of currents over a 19 day period (19 August to 6 September, 1977). The mooring was deployed in the vicinity of Ocean Weather Station P, at 49°37'N, 145°6'W, where the ocean depth is 4360 m. There were 19 vector averaging current meters (VACM's) deployed at mean depths of 5, 8, 11, 14, 20, 23, 26, 29, 32, 35, 38, 41, 44, 47, 50, 70, 92, 125, and 175 m. A vector measuring current meter (VMCM) was located at 94 m.

The VACM records current and temperature at 112.5 sec intervals (32 cph). The VACM measures the polar coordinates of the velocity field using a Savonius rotor, a vane, and a magnetic compass. In a sense, the VACM is analogous to an odometer, rather than a speedometer. Every 1/8 rotor turn (corresponding to about 4.7 cm of water displacement), the sine and cosine of the angle of the vane relative to magnetic north are accumulated in east-west and north-south registers. The registers are accumulated, and are transferred digitally to a magnetic tape (and reset) each recording interval. Later in the laboratory, the records are processed and converted into physically meaningful measurements (McCullough, 1975).

Halpern et al. (1981) performed intercomparison tests between various types of current meters and moorings deployed during MILE and JASIN (Joint Air-Sea Interaction

Project). They compared spectra between VACM's and VMCM's, and among surface toroid, spar, and torpedo buoys, and subsurface buoy moorings. From each comparison they determined a maximum usable frequency, defined as the frequency beyond which the spectra diverge. The maximum usable frequencies of the VACM's deployed in the upper 20 m ranged from 4 to 8 cph. In deeper water the maximum usable frequencies are smaller due to smaller velocity fluctuation magnitudes. During JASIN, at depths between 79 m and 92 m, maximum usable frequencies ranged from 0.2 to 8 cph. During MILE only a single estimate of the maximum usable frequency, 2 cph, was available in this depth range.

In order to eliminate the high frequency oscillations which result from mooring motions and imperfect current meter response, we have applied a low pass filter to the current meter records. We used a special FORTRAN program (Rabiner and Gold, 1975) written by Jim McClellan at Rice University to design an optimal finite impulse response filter. We designed the 128-point symmetric low pass filter to have a cutoff frequency of 2 cph and a transition band from 2 cph to 2.5 cph. The original records were sampled at 32 $hr^{-1}$, so that 1 hr of data was lost from the beginning and the end of the record. We subsampled the filtered record at 8 $hr^{-1}$ (Nyquist frequency = 4 cph). This sampling rate was deliberately chosen to be a little higher than necessary, in order to minimize possible aliasing.

Since we are interested in the probability density distributions of shear, a question arises concerning the effects of instrument nonlinearity and calibration uncertainty on the observed distributions. Briscoe (1977) considered a simple statistical model of these effects on

VACM's. From the calibration curves of McCullough (1975), he estimated that these effects will adversely affect skewness and kurtosis observations by only a few percent. He concluded that difficulties with VACM calibration uncertainty are very unlikely to be the source of observed large deviations from Gaussianity.

## 2.2 DENSITY STRATIFICATION FROM TEMPERATURE GRADIENTS

Figure 2.1 shows temperature and salinity profiles from two CTD casts on 21 and 24 August during MILE. During this period, the surface mixed layer deepened, but the main thermocline shallowed by about the same amount, and the water column above 100 m has cooled and become more saline.

Figure 2.2 shows the averaged temperature-salinity relations from CTD casts. Above 75 m (below $\sigma_t$ = 26 gm/cm$^3$), about 80% of the density gradient is due to the temperature gradient, and 20% is due to the salinity gradient. Between 100 and 150 m, virtually all of the density gradient is due to salinity.

Temperature sensors were potted within the VACM housings. Because of the thermal inertia of the housings, the temperature response is attenuated at frequencies above 1 cph (Levine, 1980). In order to produce temperature records with the same sampling intervals as those for current, we applied the same filtering process described in Section 2.1. There were no conductivity sensors attached to the current meters. Estimates of time-dependent density stratification are thus derived from the temperature sensor records alone, using mean salinity profiles, in the upper 75 m. We use an empirical formula for $\sigma_t$ from Mamayev (1975);

$$\sigma_t = 28.152-0.0735T-0.00469T^2+(0.802-0.002T)(S-35) , \quad (2.1)$$

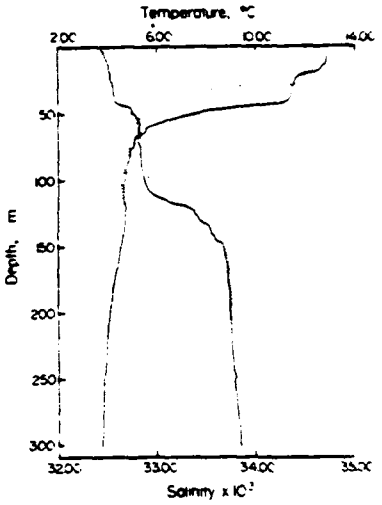


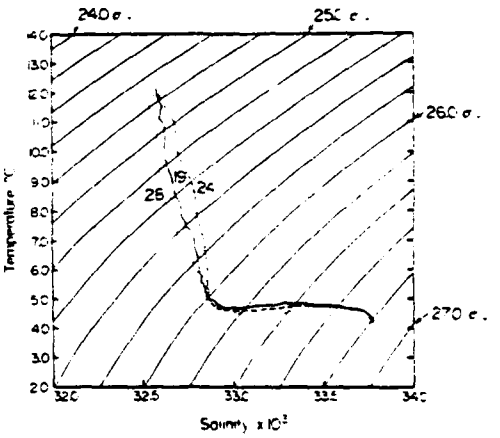


Figure 2.1 Left: Profiles of temperature and salinity at 49°35'N, 145°08'W, 0845 GMT, 21 August 1977 (solid) and 49° 38'N, 145°08'W, 1320 GMT, 24 August 1977 (dotted). From Davis et al. (1981).

Figure 2.2 Right: T-S relation from CTD casts averaged on 19 (solid), 24 (dashed), and 28 (dotted) August, 1977. The 6 September curve (not shown) closely coincides with that from 19 August. From Davis et al. (1981).

where T is temperature in °C, and S is salinity in °/oo (parts per thousand). We are interested in obtaining the density gradient.

We write

$$\frac{dS}{dz} \cong \left(\overline{\frac{dS}{dT}}\right) \frac{dT}{dz} \ , \ S \cong \overline{S} \ , \tag{2.2}$$

where $\overline{S}$ = 32.7°/oo and $(\overline{dS/dT})$ = -0.041(°/oo/°C) are representative values of salinity and salinity gradient, estimated from Figure 2.2. The density gradient becomes

$$\frac{d\sigma_t}{dz} \cong -(0.1017+0.0093T) \frac{dT}{dz} \ . \tag{2.3}$$

Then, from the definition of Vaisala frequency

$$N^2 = -\frac{g}{\rho} \frac{d\rho}{dz} \ , \tag{2.4}$$

we obtain

$$N^2 \cong (9.93+0.91T) \cdot 10^{-4} \frac{dT}{dz} \ (sec^{-2}) \ . \tag{2.5}$$

In practice, we use pairs of current meters to compute $N^2$. With two current meters 1 and 2 with vertical separation $\Delta z$, T is the average $(T_1+T_2)/2$, and dT/dz is the first difference $(T_1-T_2)/\Delta z$.

# Section 3
# TEMPORAL VARIABILITY OF SHEAR DISTRIBUTION

In this section we examine the **variability of shear.** Much of the shear variance is oscillatory at the **inertial frequency.** This is shown clearly in Figure 3.1, which shows several examples of rotary spectra of shear. The spectral peak at the local inertial frequency is the dominant spectral feature in all cases. *The inertial frequency* is $f = 2\Omega \sin \lambda$, where $\Omega$ is the earth's angular rotation rate and $\lambda$ is the latitude.

In Section 3.1 we describe the process of **complex demodulation,** and how it can be used to determine the frequency and angle of propagation of an internal wave packet. In Section 3.2 we discuss the **bimodal probability density functions** observed for inertial waves over short term intervals. As we increase the time interval of observation, the bimodal probability density becomes smeared, and within about three inertial periods, approaches Gaussianity. This result is shown in Section 3.3.

## 3.1 COMPLEX DEMODULATION

The process of complex demodulation of a shear time series can give us the temporal variability of near-inertial shear amplitude and phase. Let $U_z(t) = u_z + iv_z$ be a vector time series of shear. We seek a complex time series D(t) such that $D(t)\exp(-ift)$ most closely resembles $U_z$ in a time interval 2T centered around t, where T is the inertial period $2\pi/f$. Perkins (1970) showed that

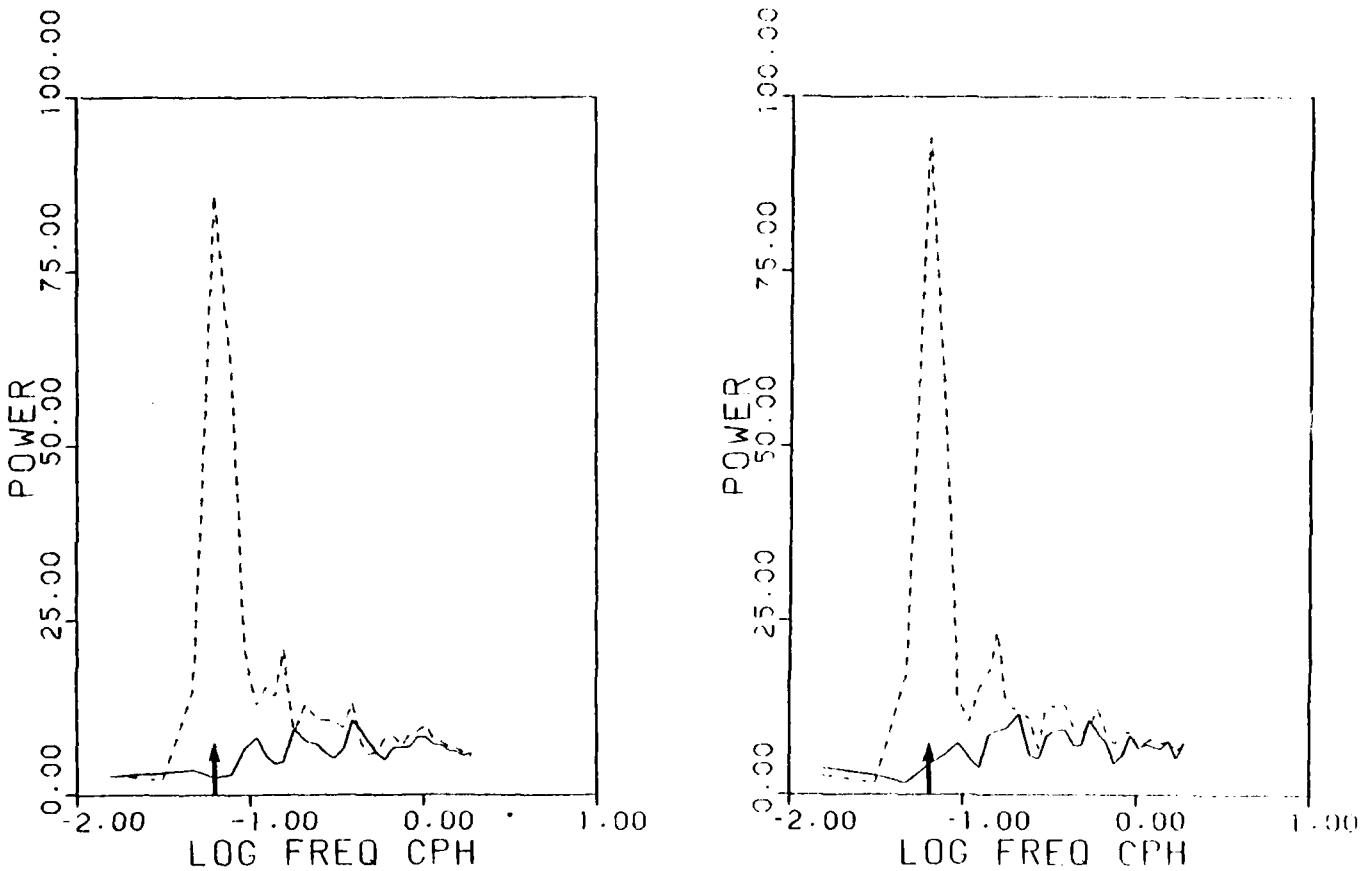


Figure 3.1 Rotary spectra of velocity difference, in variance preserving form. Left: 29-32 m, Right: 32-35 m. Dashed curves are clockwise and solid curves are counterclockwise rotary power. Vertical axes have units $cm^2/sec^2$. Arrows point at inertial frequency.

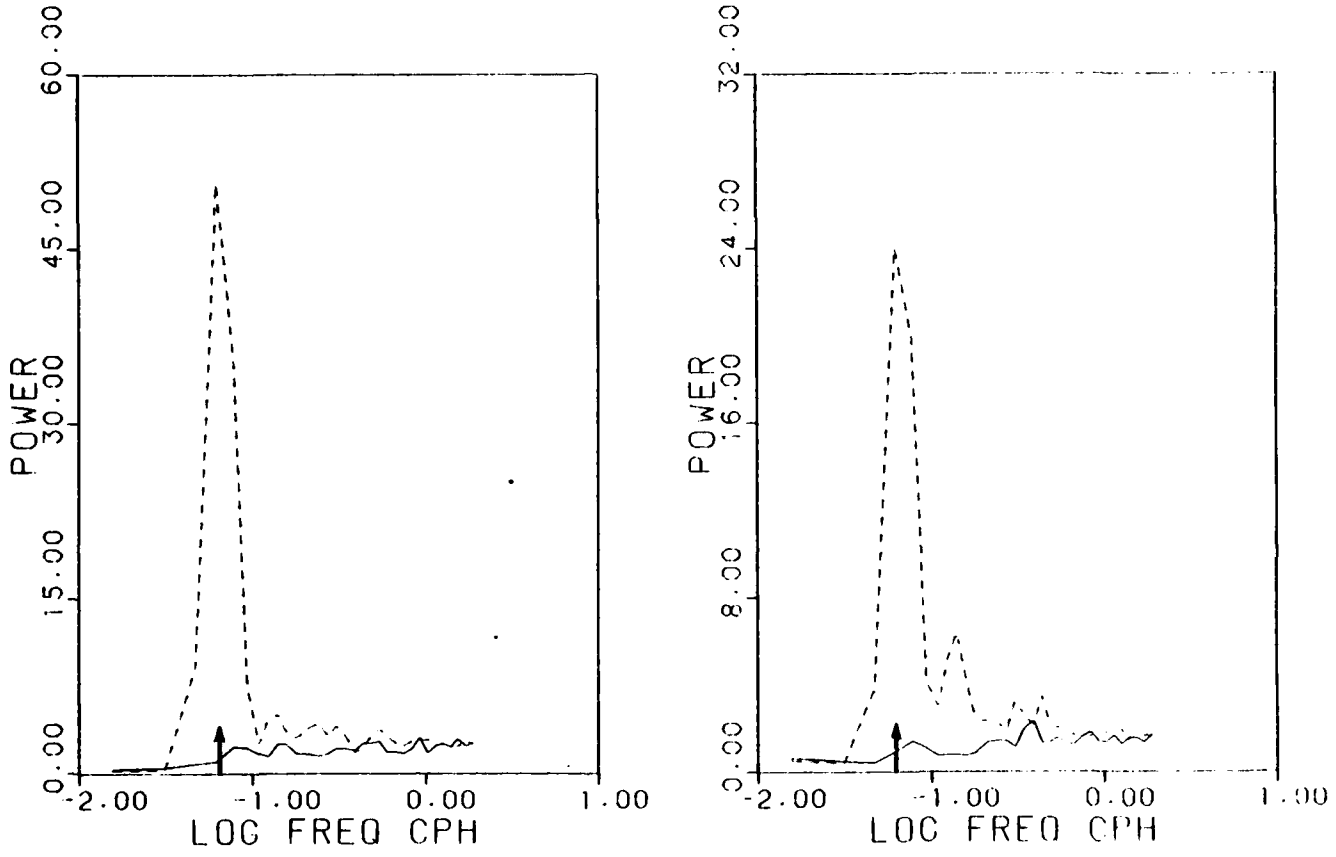


Figure 3.1, continued: Rotary spectra of velocity difference, in variance preserving form. Left: 41-44 m, Right: 44-47 m. Dashed curves are clockwise and solid curves are counter-clockwise rotary power. Vertical axes have units $cm^2/sec^2$. Arrows point at inertial frequency.

$$D(t) = \frac{1}{2T} \int_{t-T}^{t+T} \exp(ift)\, U_z(t)\, dt \ . \qquad (3.1)$$

Thus, $|D|$ and $\arg(D)$ are the amplitude and phase of inertial shear at time t. Figure 3.2 is an example of complex demodulated velocity difference between 29 and 32 m. The dashed curve is the amplitude and the solid curve is the phase. A slow decrease in phase with time corresponds to a frequency slightly higher than inertial. For example, between days 4 and 8, the amplitude increases but slowly, while the phase decreases by about 120°. This corresponds to a frequency increment $\Delta\omega$ = .003 cph, giving a total frequency $f + \Delta\omega$ = .067 cph, about 5% higher than f. This frequency increment is of the same order as observed by others (e.g., Kundu, 1976).

In order that internal waves be able to propagate, their frequency $\omega$ must be in the range $f < \omega < N$. As $\omega$ decreases toward f, the group velocity vector approaches the horizontal direction, and the vertical component vanishes at $\omega = f$. The angle of propagation $\theta$ of the group velocity vector with respect to the horizontal is approximately

$$\theta \approx \frac{f}{N(z)} \sqrt{2(\omega/f - 1)} \ , \qquad (3.2)$$

where the assumptions $\omega - f << f << N(z)$ have been made (see Rubenstein, 1981). In the present case illustrated from days 4 to 8 in Figure 3.2, the rms value of N(z) is 0.023 $sec^{-1}$. Therefore the angle of propagation is $1.6 \times 10^{-3}$ rad, or about 0.1°.

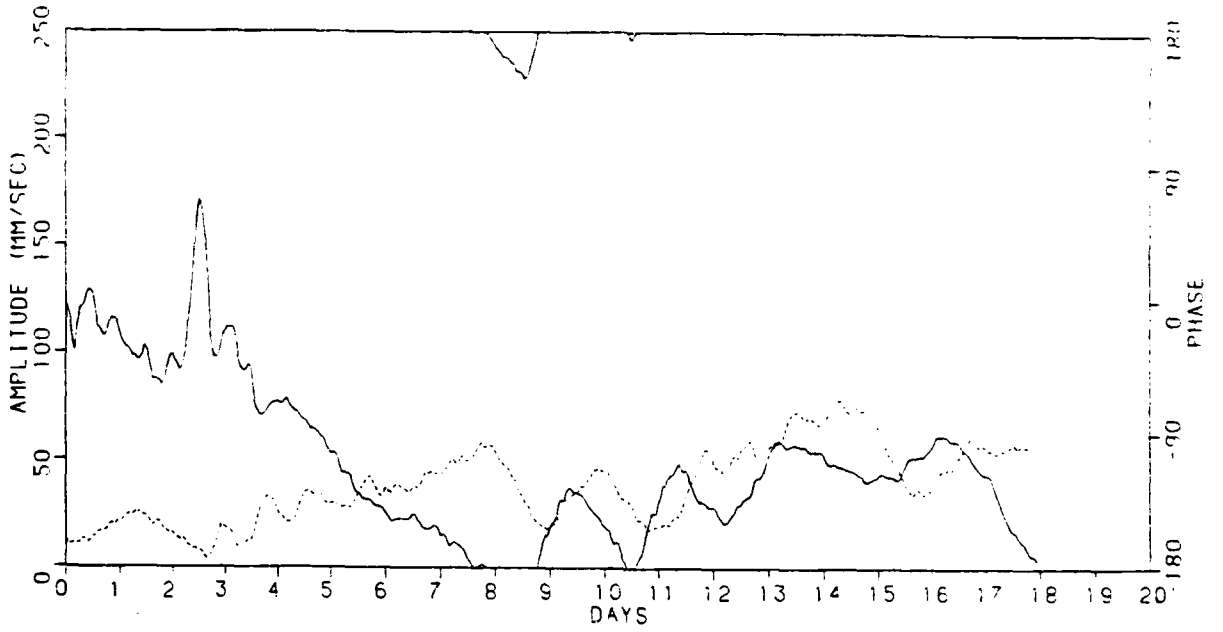


Figure 3.2 Complex demodulation of velocity difference between 29 and 32 m. Dashed curve: amplitude, solid curve: phase. When the slope in phase is positive (negative) the frequency is lower (higher) than the inertial frequency. From equation (3.1) in the text.

## 3.2 DISTRIBUTION OF INERTIAL OSCILLATIONS

Over time scales of order one inertial period, the probability density of shear is a bimodal distribution, while over much longer time scales, the probability density approaches that of a Gaussian distribution. In an ideal case with a constant amplitude inertial oscillation with zero phase shift, the shear vector traces out a circular pattern. Each shear component has a bimodal probability density function. With the introduction of a component of higher frequency shear, the circular pattern becomes smeared. If the amplitude of the inertial oscillations varies slowly, then this low frequency component of shear smears the circular pattern still further. If these "noise" components are sufficiently strong, then over the course of several inertial periods, the probability density function approaches Gaussianity.

We can examine this process by developing a simple statistical model of "noisy" inertial shear. We begin with the ideal case, by stipulating that the shear vector oscillates in a circle, and each of the shear components oscillate sinusoidally, but out of phase by $\pi/2$. For example, let

$$x_i = X_i \sin ft \tag{3.3}$$

be the $u_z$ component of inertial shear, where $X_i$ is the amplitude of the oscillation. Then it is easy to show that the probability density function is

$$f(x_i) = \begin{cases} \dfrac{1}{\pi\sqrt{X_i^2 - x_i^2}} & |x_i| \leq X_i \\ 0 & |x_i| > X_i \,. \end{cases} \tag{3.4}$$

Now suppose that we add to this inertial shear an extra "noise" component $x_n$. We let this component have a uniform density function:

$$g(x_n) = \begin{cases} 1/(2X_n) & |x_n| \leq X_n \\ 0 & |x_n| > X_n. \end{cases} \qquad (3.5)$$

We are interested in the probability density h of the total shear $x = x_i + x_n$. We compute h by performing the following integral;

$$h(x) = \int_{-\infty}^{\infty} f(x-x_n)\, g(x_n) dx_n. \qquad (3.6)$$

We combine equations (3.4)-(3.6) and after a bit of algebra we obtain a symmetric probability density function. The **positive** side of this function is written as follows;

$$h(x) = (2\pi X_n)^{-1} \left[ \sin^{-1}\left(\frac{X_n - x}{X_i}\right) + \sin^{-1}\left(\frac{X_n + x}{X_i}\right) \right] \qquad (3.7a)$$

in the range $0 \leq x \leq X_i - X_n$, and

$$h(x) = (2\pi X_n)^{-1} \left[ \sin^{-1}\left(\frac{X_n - x}{X_i}\right) + \frac{\pi}{2} \right] \qquad (3.7b)$$

in the range $X_i - X_n \leq x \leq X_i + X_n$. Figure 3.3 shows h(x) for $X_i = 1$, $X_n = 0.1$, 0.3, and 1.0. For $X_n = 0.1$, the probability density function is strongly bimodal; the two cusps are at $x = \pm (X_i - X_n)$. As $X_n$ increases, the cusps approach each other, and converge when $X_n = 1$; that is to say, the distribution becomes unimodal.

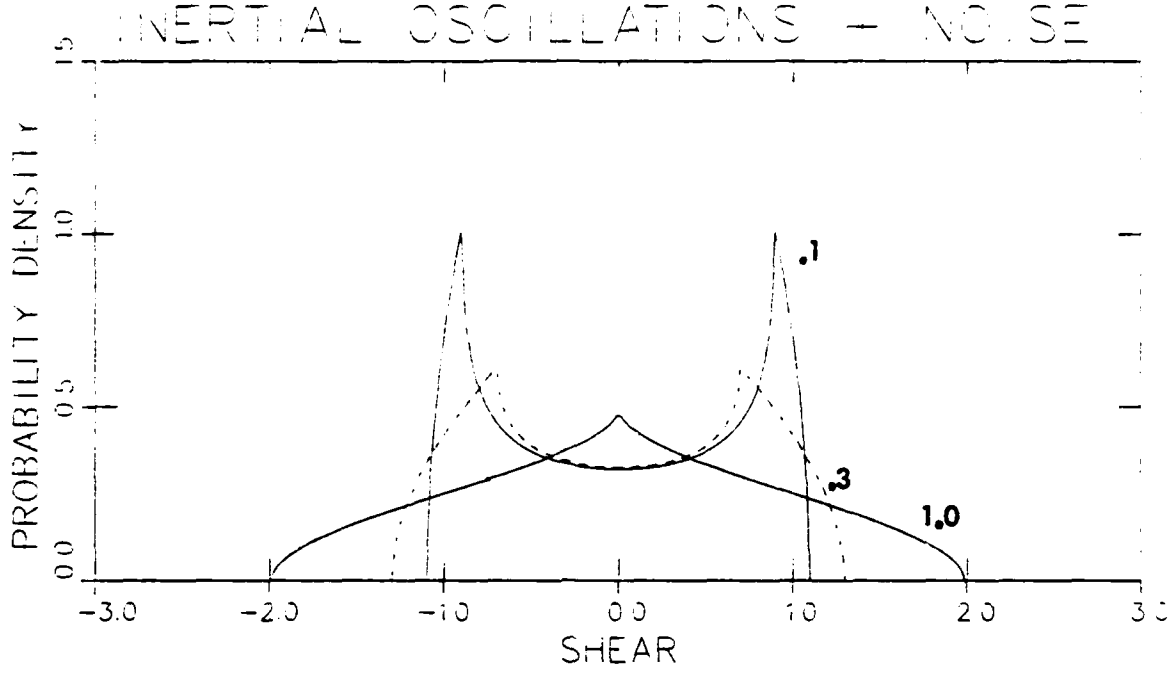


Figure 3.3 Probability density functions h(x) given by equation (3.7). The ratios $X_n/X_i$ = 0.1, 0.3, and 1.0 are proportional to the ratio of the variances of the noise and inertial oscillation distributions.

Over a short duration, this model is often a reasonable approximation to the observed probability density. Figure 3.4 shows a trace of the vector of velocity difference between 26 and 38 m, over an inertial period (~16 hours). The trace appears to be approximately circular, with seemingly random noise superimposed. Figure 3.5 shows the distribution of the u-component of this vector time series. The agreement with the model probability density function from (3.7), with $X_n = 0.3$, appears to be very good. We do not attempt to optimize or to quantify this agreement. We only wish to point out that the observed distribution is bimodal, and can be understood on a qualitative level as the combination of the "oscillatory" distribution (3.4) and the uniform distribution (3.5). In most of the cases where shear component time series were analyzed over an inertial period, the distributions were found to be bimodal. However, in many cases the distributions did not compare favorably with (3.7), because the distributions had significantly large skewness levels. In these cases, non-inertial frequency components were significant.

## 3.3 LONG-TERM GAUSSIAN DISTRIBUTION

Over a duration of several inertial periods, low frequency shear components accumulate and tend to smear out the bimodal distributions. A duration of three inertial periods is sufficient, generally, to generate nearly Gaussian distributions. We have analyzed the skewness, kurtosis, and Lilliefors test statistic for 48 hr shear distributions over $\Delta z = 3$ m. The 48 hr interval is almost exactly three 15.7 hr inertial periods. The shear was sampled at 4 hr intervals, in order to achieve statistically independent samples. Section 5.1.1 presents the rationale for this choice. Also,

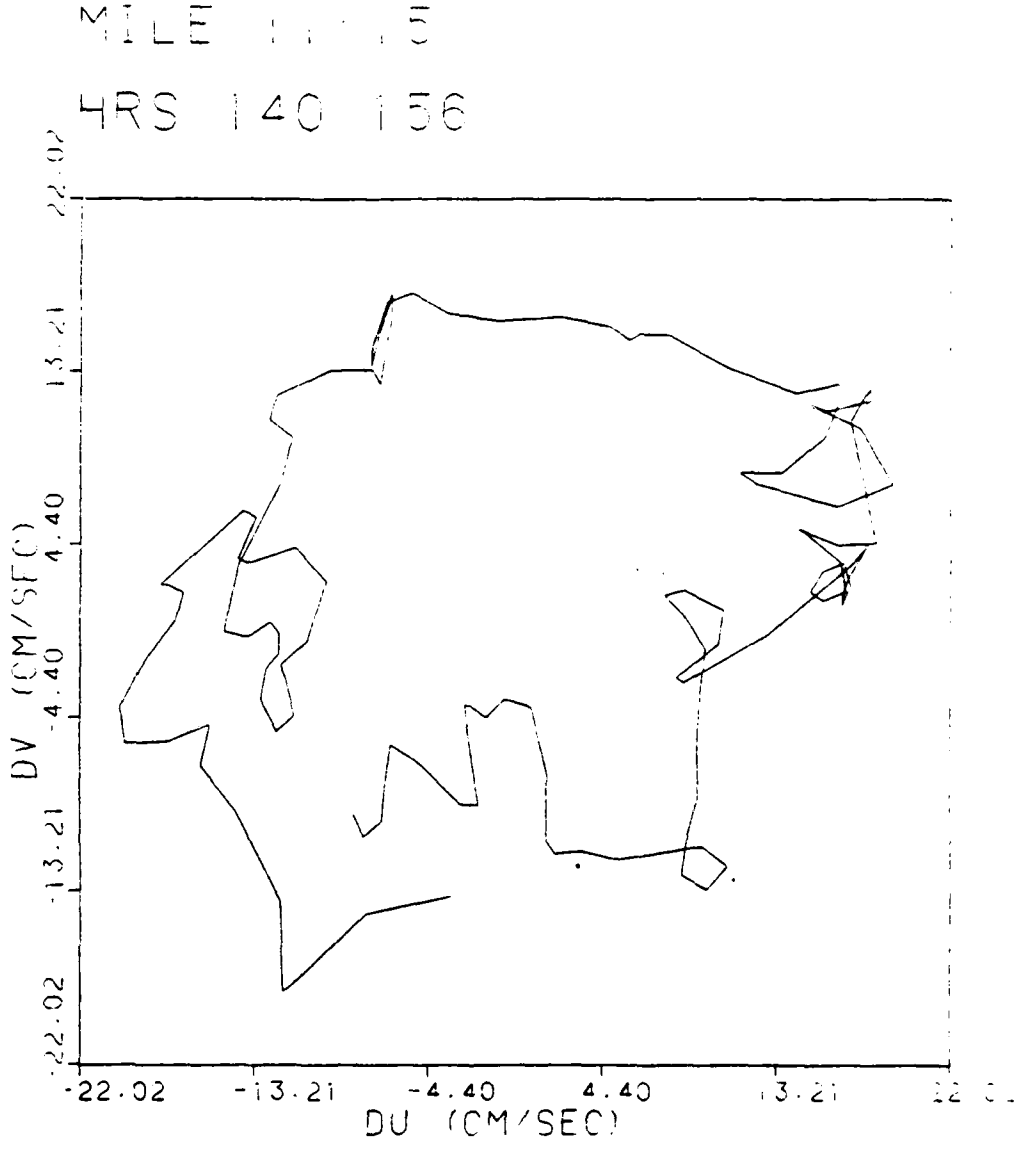


Figure 3.4 Vector trace of velocity difference between depths 26 and 38 m, during an inertial period, about 16 hours. Over the course of an inertial period, the trace is approximately circular, with higher frequency fluctuations superposed.

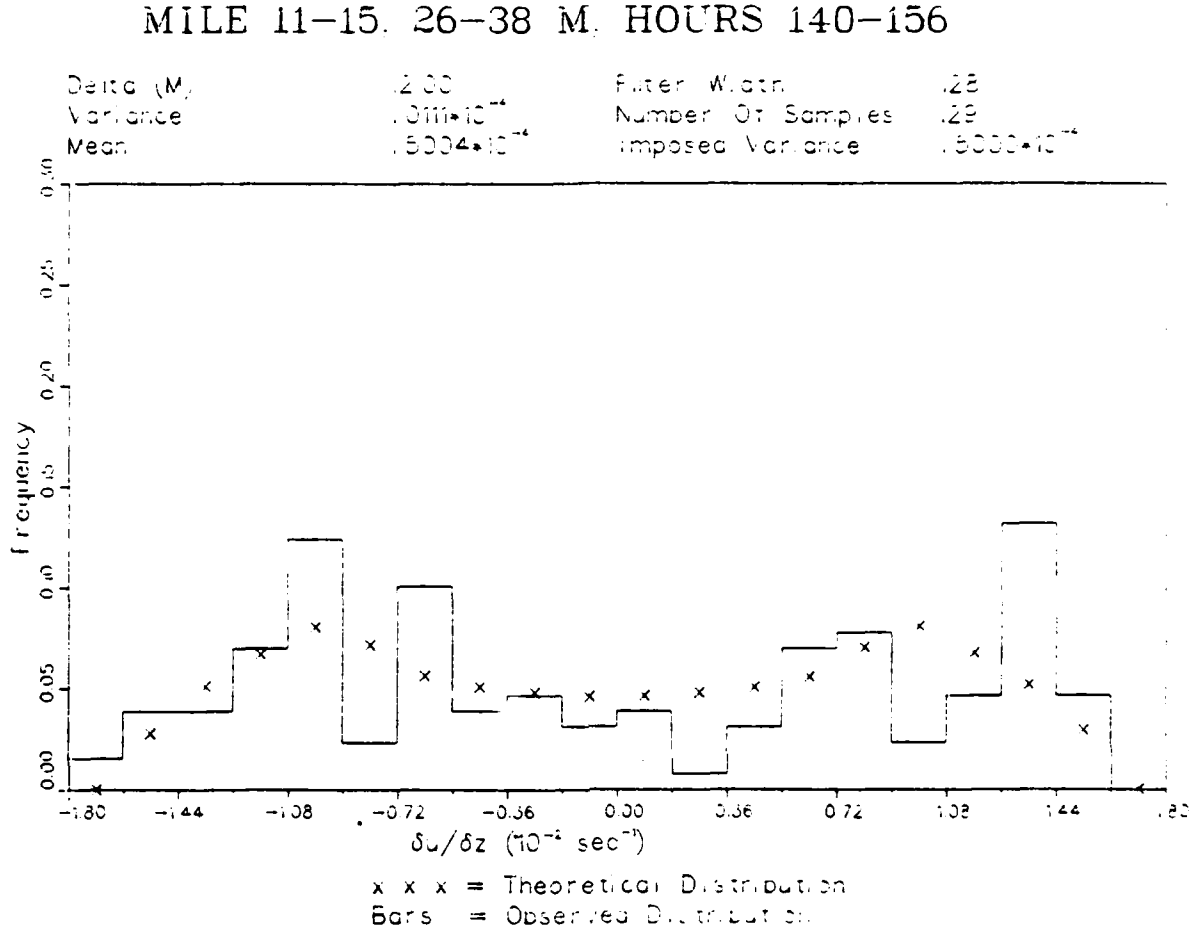


Figure 3.5 Shear distribution over depth interval 26-38 m, over an inertial period, about 16 hours. The theoretical distribution function from equation (3.7) is bimodal, with $X_n = 0.3$. The fit has not been optimized, but does appear to be reasonable.

we refer the reader to Section 5.2 for a discussion of the Lilliefors test for Gaussianity. Skewness is defined as $\Sigma(x_i-\bar{x})^3/N\sigma^3$, and kurtosis is defined as $\Sigma(x_i-\bar{x})^4/N\sigma^4$, where $\bar{x} = \Sigma x_i/N$ and $\sigma^2 = \Sigma(x_i-\bar{x})^2/N$ are the mean and variance, respectively. The expected skewness of a Gaussian distribution (as well as any symmetric distribution) is zero. The expected kurtosis of a Gaussian distribution is 3. For this reason, we have subtracted 3 from each kurtosis statistic.

Figure 3.6 shows an example of the analysis results. This example has been selected to be representative of the entire body of results. With but few exceptions, skewness and kurtosis-3 oscillate about zero, within the limits $\pm 1.5$. The test statistic generally falls below 0.24, the 95% confidence ($\alpha = .05$) level. The implication is that these short samples come from a population which may reasonably be approximated as a Gaussian distribution.

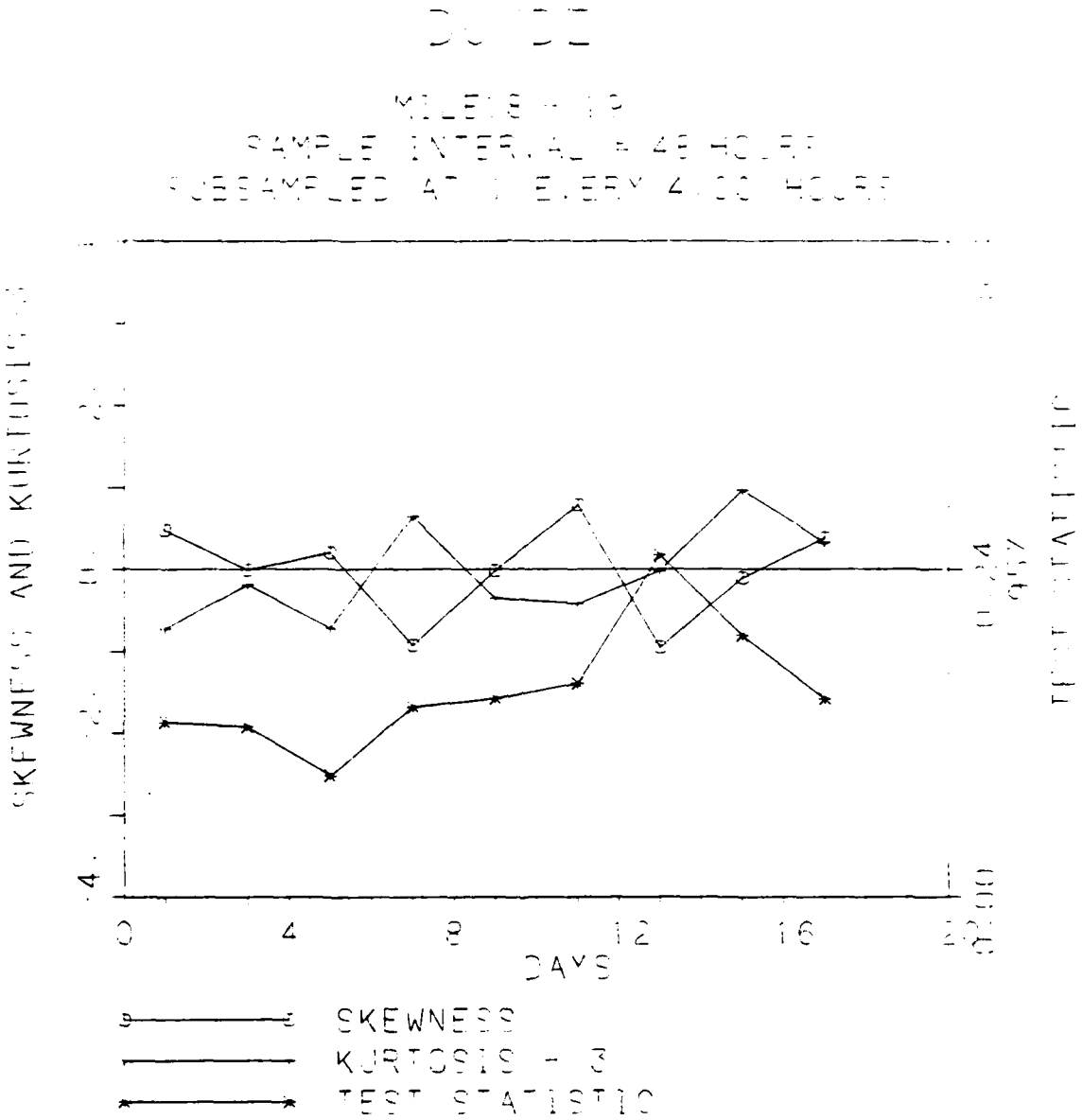


Figure 3.9 Skewness, kurtosis-3, and Lilliefors test statistic for Gaussianity, for 48-hr records of shear component du/dz over depth interval 47-50 m. The horizontal line indicates the 95% confidence level for the test statistic.

## Section 4
## STATISTICAL MODEL OF MEAN-SQUARE SHEAR

In this section we derive a simple spectral model of shear to predict how measurements of mean-square shear vary with the vertical separation $\Delta z$ between current meters. This analysis is largely taken from Grabowski (1981), but the deviation is slightly different. Then we compare these predictions with measurements in the seasonal thermocline from the MILE-1 current meters. The comparison is favorable, and lends support to the composite shear spectrum of Gargett et al. (1981), upon which our model is based.

### 4.1 *PREDICTIONS OF MEAN-SQUARE SHEAR*

We begin by representing the complex valued velocity field $U(z) = u(z) + iv(z)$ as a Fourier integral

$$U(z) = \int_{-\infty}^{\infty} U(k)\ e^{ikz}\ dk\ , \qquad (4.1)$$

where k is the vertical wavenumber. The one-sided velocity power spectral density function (defined over positive k) is

$$P_u(k) = 2\langle U(k)U^*(k)\rangle\ , \qquad (4.2)$$

where the brackets denote an ensemble average.

Suppose we were to sample U(z) at discrete intervals, and estimate the shear $S(z;\Delta z)$ by performing a first differencing operation;

$$S(z;\Delta z) = \frac{U(z+\Delta z) - U(z)}{\Delta z}\ . \qquad (4.3)$$

Taking the Fourier transform of (4.3) we get

$$S(k;\Delta z) = \frac{-2iU(k)}{\Delta z} \exp(-ik\Delta z/2) \sin(k\Delta z/2) \ . \quad (4.4)$$

Therefore, the power spectral density of shear $P_s(k;\Delta z)$ over a finite interval $\Delta z$ is

$$P_s(k;\Delta z) = 4P_u(k) \left(\frac{\sin(k\Delta z/2)}{\Delta z}\right)^2 \ . \quad (4.5)$$

In the limit as $\Delta z$ goes to zero,

$$P_s(k) = \lim_{\Delta z \to 0} P_s(k;\Delta z) = k^2 P_u(k) \ . \quad (4.6)$$

In Figure 4.1 we illustrate a shear spectrum model $P_s(k)$, after the composite spectrum by Gargett et al. The form of this model is

$$P_s(k) = \begin{cases} N^2/k_o & k \leq k_o \\ N^2/k & k_o \leq k < k_b, \end{cases} \quad (4.7)$$

where N is the local Vaisala frequency, $k_o$ is taken as 0.1 cpm, and the buoyancy wavenumber, $k_b$, is taken as 1 cpm. We do not include contributions from the high wavenumber turbulence dissipation range in this model. We substitute (4.6) and (4.7) into (4.5) and integrate over wavenumber to obtain the expected value of mean square shear;

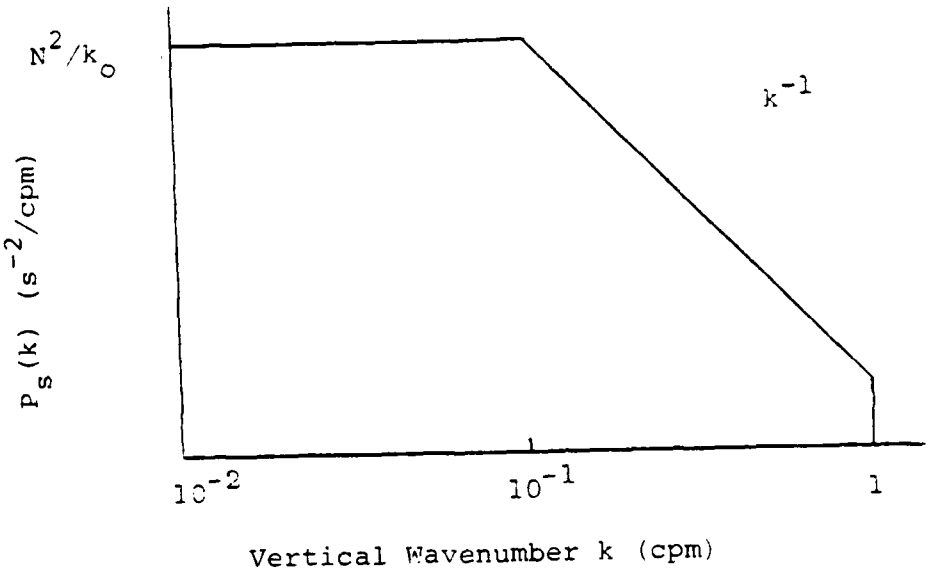


Figure 4.1 Idealized shear spectrum after Gargett et al. (1981). The rolloff wavenumber is $k_o$ = .1 cpm, and the buoyancy wavenumber is $k_b$ = 1 cpm.

$$\langle |S(z;\Delta z)|^2 \rangle = N^2/k_o \int_0^{k_o} \left[\frac{\sin(k\Delta z/2)}{k\Delta z/2}\right]^2 dk$$

$$+ N^2 \int_{k_o}^{k_b} k^{-1} \left[\frac{\sin(k\Delta z/2)}{k\Delta z/2}\right]^2 dk. \qquad (4.8)$$

Writing $y = k\Delta z/2$, $y_o = k_o \Delta z/2$, and $y_b = k_b \Delta z/2$, (4.8) becomes

$$\langle |S(z;\Delta z)|^2 \rangle = \frac{2N^2}{\Delta z k_o} \int_0^{y_o} \frac{\sin^2 y}{y^2} dy + N^2 \int_{y_o}^{y_b} \frac{\sin^2 y}{y^3} dy \qquad (4.9)$$

Grabowski (1981) evaluated the first integral $I_1$ in (4.9);

$$I_1 = \frac{\cos 2y_o - 1}{2y_o} + Si(2y_o) \qquad (4.10)$$

and the second integral $I_2$ is

$$I_2 = \frac{1}{4}\left[y_b^{-2}(\cos 2y_b - 1) - 2y_b^{-2} \sin 2y_b \right.$$

$$\left. -y_o^{-2}(\cos 2y_o - 1) + 2y_o^{-1} \sin 2y_o \right]$$

$$-Ci(2y_o) + Ci(2y_b) , \qquad (4.11)$$

where

$$Si(x) = \int_0^x t^{-1} \sin t \, dt$$

and

$$Ci(x) = -\int_{x}^{\infty} t^{-1} \cos t \, dt \qquad (4.12)$$

are the sine and cosine integrals. Model predictions of normalized mean-square velocity differences

$$\frac{\langle |S(z;\Delta z)|^2 \rangle \Delta z^2 k_o}{2N^2} = \Delta z(I_1 + k_o \Delta z I_2/2) \qquad (4.13)$$

are tabulated in Table 4.1. From Table 4.1 it is evident that mean square velocity differences become asymptotically proportional to $\Delta z$ for large $\Delta z$. In the next section, we present a graph of the relationship (4.13), and compare with the values of mean-square velocity differences from the MILE current data.

Table 4.1
Mean-Square Velocity Differences

| $\Delta z$ (m) | $\langle \lvert S(z;\Delta z) \rvert^2 \rangle \Delta z^2 \, k_o/2N^2$ |
|---|---|
| 2 | 2.15 |
| 4 | 4.84 |
| 6 | 8.17 |
| 8 | 11.39 |
| 10 | 14.32 |
| 12 | 17.24 |
| 14 | 20.40 |
| 16 | 23.70 |
| 18 | 26.89 |
| 20 | 29.92 |

## 4.2 STATISTICAL MODEL-DATA COMPARISONS

In this section we compare mean-square shear with our model prediction. We begin by showing that $\overline{S^2}$, computed from current meters over each of four different vertical separations $\Delta z$, is linearly proportional to $\overline{N^2}$. The overbars denote temporal averages over a 19-day period. Using the method of least-squares, we compute estimates of the normalized mean-square velocity difference $k_o(\overline{S^2}/2\overline{N^2})\Delta z^2$, as a function of $\Delta z$. Finally we compare these results with the statistical model prediction (4.13).

Figures 4.2-4.5 show observed values of $\overline{S^2}$ as functions of $\overline{N^2}$, for $\Delta z$ = 3, 6, 12, and 21 m. Mean-square total shear $\overline{S^2}$ is denoted by triangles, and is plotted against the left-hand axes. The individual components of mean-square shear, $\overline{(\Delta u/\Delta z)^2}$ and $\overline{(\Delta v/\Delta z)^2}$, are plotted on twice the scale as the total mean-square shear. The dashed lines show the origin-forced least-squares best fits; $\overline{S^2} = b\overline{N^2}$. In each figure, the correlation coefficient is better than 0.99.

Table 4.2 lists the coefficients b of the least-squares regressions for each value of $\Delta z$. The value of b decreases with $\Delta z$, and is approximately proportional to $\Delta z^{-1}$. That is to say, mean-square shear becomes proportional to $\Delta z^{-1}$, and mean-square velocity differences $S^2\Delta z^2$ become proportional to $\Delta z$, for large $\Delta z$.

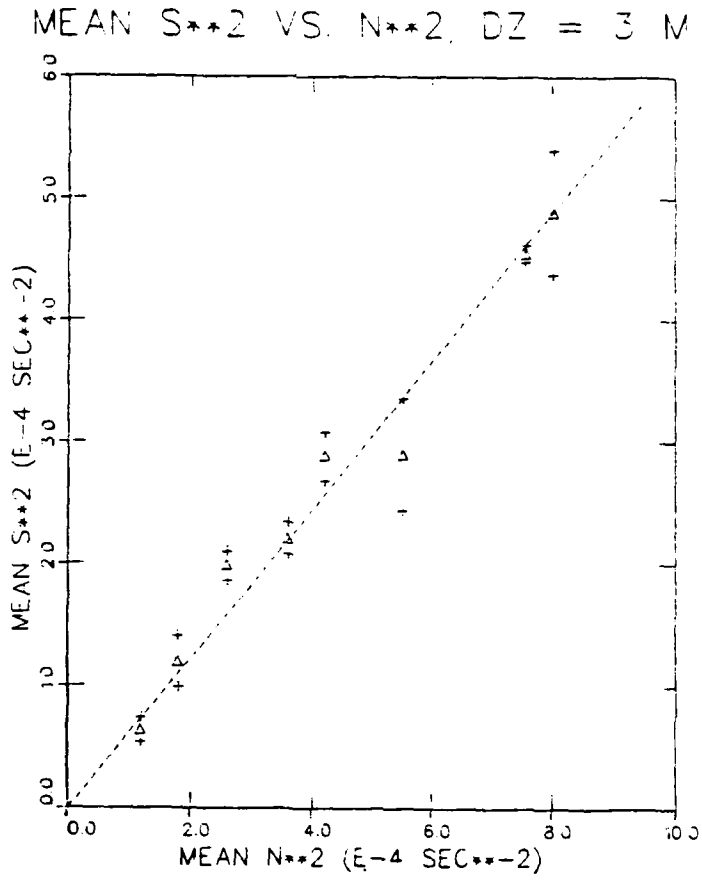


TRIANGLES: TOTAL $\overline{S^2}$

CROSSES: 2x $\overline{(DU/DZ)^2}$, $\overline{(DV/DZ)^2}$

DASHED LINE: $\overline{S^2} = 0.61\overline{N^2}$

Figure 4.2 $\overline{S^2}$ vs. $\overline{N^2}$ from eight pairs of current meters in the depth range 26-50 m, with $\Delta z$ = 3 m. Individual shear components (crosses) are plotted on twice the scale of the total $S^2$ (triangles). Dashed line is best fit through the triangles.

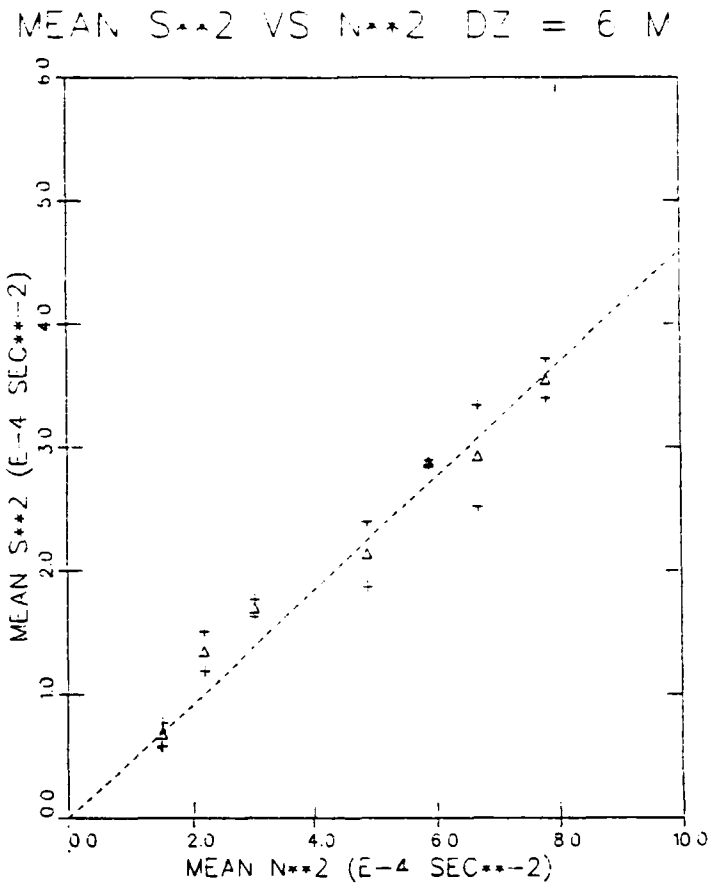


TRIANGLES: TOTAL $\overline{S^2}$

CROSSES: 2x $\overline{(DU/DZ)^2}$, $\overline{(DV/DZ)^2}$

DASHED LINE: $\overline{S^2} = 0.46\overline{N^2}$

Figure 4.3 $\overline{S^2}$ vs. $\overline{N^2}$ from seven pairs of current meters in the depth range 26-50 m, with $\Delta z$ = 6 m. Individual shear components (crosses) are plotted on twice the scale of the total $\overline{S^2}$ (triangles). Dashed line is best fit through the triangles.

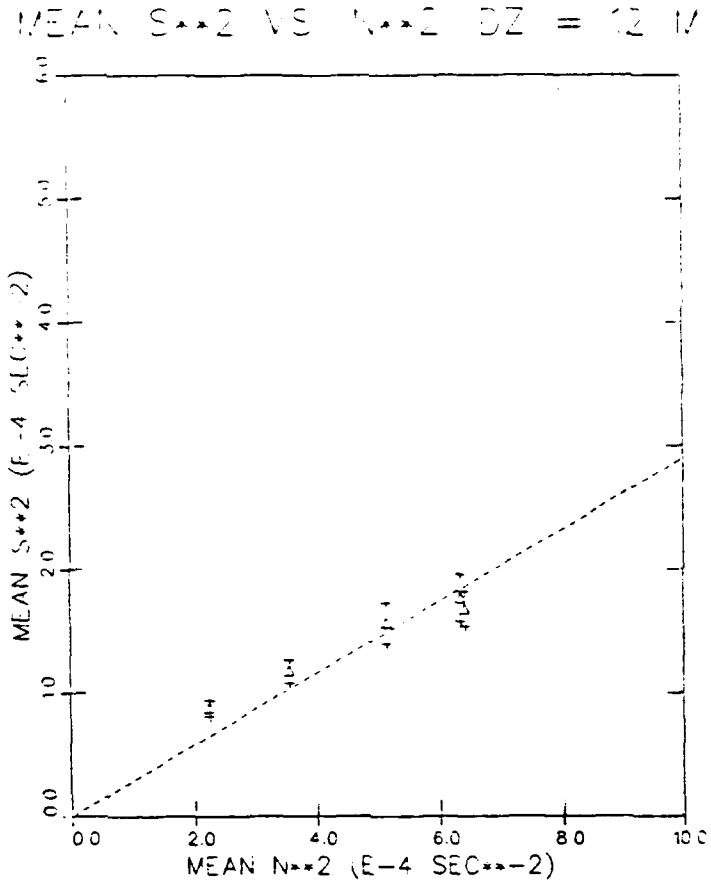


TRIANGLES: TOTAL $\overline{S^2}$

CROSSES: $2x\ \overline{(DU/DZ)^2}.\ \overline{(DV/DZ)^2}$

DASHED LINE: $\overline{S^2} = 0.29\overline{N^2}$

Figure 4.4 $\overline{S^2}$ vs. $\overline{N^2}$ from five pairs of current meters in the depth range 26-50 m, with $\Delta z$ = 12 m. Individual shear components (crosses) are plotted on twice the scale of the total $S^2$ (triangles). Dashed line is best fit through the triangles.

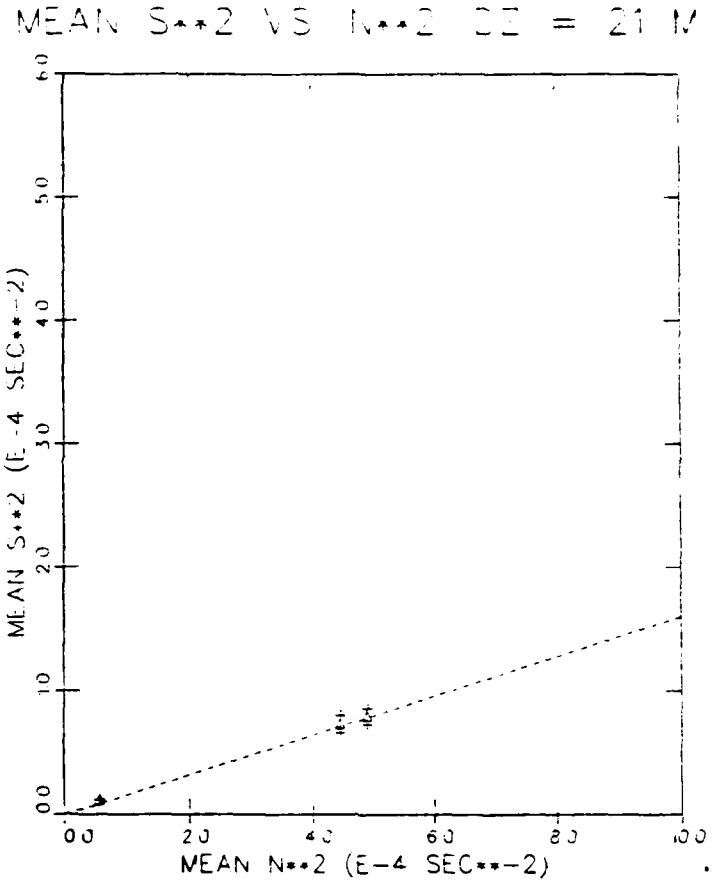


TRIANGLES: TOTAL $\overline{S^2}$

CROSSES: 2x $\overline{(DU/DZ)^2}$, $\overline{(DV/DZ)^2}$

DASHED LINE: $\overline{S^2} = 0.15\overline{N^2}$

Figure 4.5 $\overline{S^2}$ vs. $\overline{N^2}$ from three pairs of current meters in the depth range 26-70 m, with $\Delta z \approx 21$ m. Individual shear components (crosses) are plotted on twice the scale of the total $S^2$ (triangles). Dashed line is best fit through the triangles.

Table 4.2
Least-Squares Regression Coefficients $\overline{S^2} = b\overline{N^2}$

| $\Delta z$ (m) | $b = \overline{S^2}/\overline{N^2}$ | $b\Delta z^2 = (\overline{S^2}/\overline{N^2})\Delta z^2$ | $\frac{k_o\overline{S^2}}{2\overline{N^2}}\Delta z^2$ |
|---|---|---|---|
| 3 | 0.61 | 5.49 | 1.72 |
| 6 | 0.46 | 16.56 | 5.20 |
| 12 | 0.29 | 41.76 | 13.12 |
| 21 | 0.16 | 70.56 | 22.17 |

This result is analogous to that predicted by the statistical model, eq. (4.13). Figure 4.6 shows the statistical model of mean-square velocity differences (solid curve), the model times the factors $2^{\pm 1/2}$ (dashed), and observed values (triangles). The error bars indicate $\pm 2$ standard deviations, and represent the uncertainties in the coefficients b. The model prediction is greater than the observed values. Both the model and the observed values of mean-square velocity difference increase approximately linearly with $\Delta z$, with slopes 1.5 and 1.16, respectively.

Several possible explanations may be advanced for this discrepancy. The model may be overestimating the low wavenumber ($k \leq k_o$) spectral level, $N^2/k_o$. As the energy level of internal waves is universal within a factor of two (Munk, 1982), and much of the shear variance is due to low frequency internal waves, it is reasonable to expect shear spectral level to vary by a similar factor. The dashed curves in Fig. 4.6 show the statistical model predictions with the shear level adjusted by the factors $2^{\pm 1/2}$.

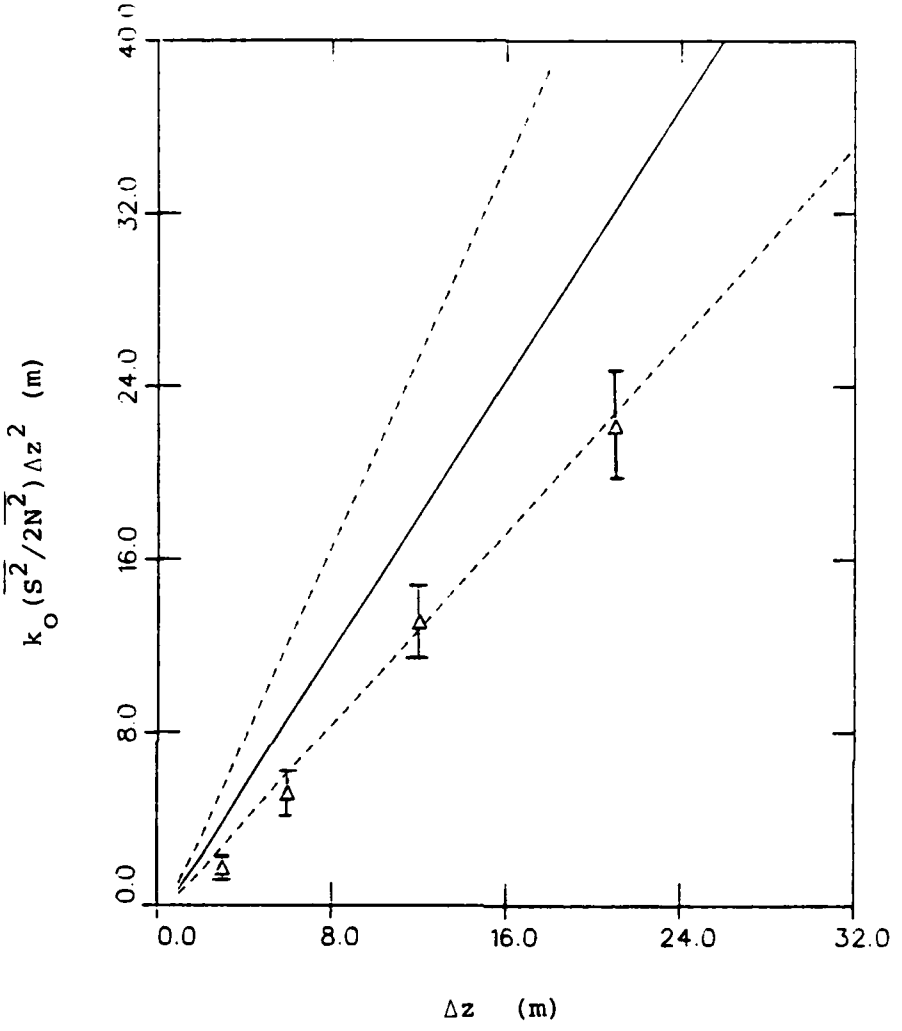


Δ = OBSERVED

—— = MODEL

--- = $\left(2^{\pm 1/2}\right)$ MODEL

Figure 4.6 Normalized mean-square velocity difference, as a function of vertical separation. The observations are based on MILE current meter pairs in the seasonal thermocline, in the depth range 26-70 m. The dashed curves show the model adjusted by the factors $2^{\pm 1/2}$.

The assumed shape of the shear spectrum may not be exact. Gargett et al. (1981) estimate the spectral roll-off wavenumber $k_o$ to be 0.1 cpm, and claim this number to be correct within a factor of two. However, our statistical model is not sensitive to changes in $k_o$, and varying $k_o$ by a factor of two will not produce better agreement with the observations. Gargett et al. mention that the low wavenumber portion of the shear spectrum might not be truly flat, and that Sanford suggests a change in spectral slope from $k^0$ to $k^{-.5}$ around $k \approx .02\text{-}.03$ cpm. If this spectral shape were correct, then the low-wavenumber portion of the spectrum would gain in relative importance. As a result, the model's prediction of mean-square shear would increase preferentially for large values of $\Delta z$.

Another possibility is that $\overline{N^2}$ is not computed correctly. We assumed in Section 2.2 that fluctuations in salinity gradient are nearly proportional to fluctuations in temperature gradient, and that the salinity gradient's contribution to the total density gradient is small. If this assumption is not valid, then our estimate for $\overline{N^2}$ may be faulty. For example, if the fluctuations in salinity gradient were less extreme than those in temperature gradient, then we have overestimated $\overline{N^2}$.

Yet another possible explanation for the discrepancy lies in the fact that $N^2$ is a strongly varying function of depth z. When $\Delta z$ is as large as 21 m, the **local** values of $N^2$ at depths z and $z+\Delta z$ may differ significantly from the **average** value over this depth range. This may cause a problem since $S^2$ is normalized by the average value of $N^2$.

Our statistical model provides a framework for obtaining information about the vertical length scales of shear from current meter time series. There is good qualitative agreement between values of shear computed from current meter time series and those computed from the statistical model. The model is derived from a vertical wavenumber spectrum which, in turn, is based on vertical profiles. This is important because it is difficult to compute reliable vertical wavenumber shear spectra from vertical profiles in the statistically nonstationary regime of the seasonal thermocline.

# Section 5
# PROBABILITY DISTRIBUTION OF SHEAR

In this section we show that shear distribution, over a time interval long compared to an inertial period, may be reasonably approximated by a Gaussian function. In Section 5.1 we show that shear time series should be sampled at 4 hr intervals (1/4 inertial period) in order to obtain statistically independent (uncorrelated) samples. We also show, using the Smirnov test, that the samples of $\Delta u/\Delta z$ and $\Delta v/\Delta z$ shear components come from parent populations whose distributions are identical.

In Section 5.2 we use the Lilliefors test to show that $\Delta u/\Delta z$ and $\Delta v/\Delta z$ have distributions that are approximately Gaussian. Then in Section 5.3 we apply the Kolmogorov test. We show that the $\Delta u/\Delta z$ and $\Delta v/\Delta z$ distributions agree well with the **particular** Gaussian distributions whose variance parameters are based on the statistical model for $\overline{S^2}(\overline{N^2},\Delta z)$ from Section 4.

## 5.1 PRELIMINARY STATISTICAL TESTS

### 5.1.1 Autocorrelation and Run Test for Randomness

In order to perform quantitative statistical tests on the shear probability distribution, we must first realize and account for the fact that shear measurements are not independent, but are autocorrelated. We use two methods to determine autocorrelation lag interval. The first method involves estimating this interval directly from shear autocorrelation functions, and the second involves the use of the run test.

In general, shear in the shallowest region of the seasonal thermocline rapidly becomes uncorrelated, while shear in the slightly deeper regions remains correlated for a length of time of order one inertial period. Figures 5.1 and 5.2 are two examples of autocorrelation functions of shear between current meter pairs at depths 29-32 m and 41-44 m, respectively. In Figure 5.1, the shear quickly becomes uncorrelated. After a lag of 1 hour, the shear reaches half-correlation. At larger lags, the function continues to oscillate at the inertial frequency. The amplitude of these oscillations is about $\pm$ 0.2. Figure 5.2 shows a somewhat different behavior. The inertial frequency oscillations decay more slowly, and reach half-correlation after a lag of about 20 hours. These examples have been chosen to be representative of the entire body of results.

In all of the autocorrelation results, the shear autocorrelation function first passed through zero at a lag of about 4 hours. This result is obvious; since inertial oscillations are an important component of the shear, the signal reaches zero correlation after 1/4 of an inertial period (15.66 hours), or about 4 hours.

A second test was also used to ascertain the degree of randomness; the run test. We individually apply this test to each of the horizontal components of vertical shear. We begin this test by subtracting the mean values from both shear components. A run is defined as a sequence of either positive or negative-valued shear observations that is followed by observations of the opposite sign (or no observation at all). The total number of runs in a time series gives us an indication of its randomness. We searched for the minimum subsampling interval for which the run test hypothesis could be accepted, consistently, at the $\alpha$ = 0.20 significance

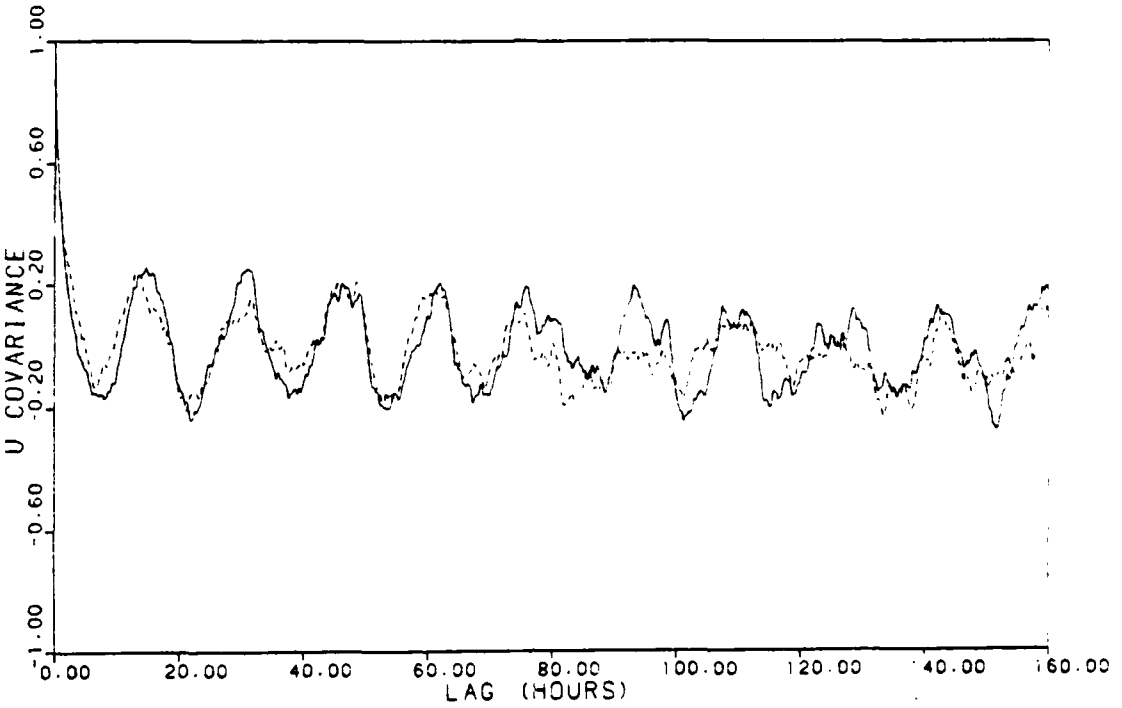


Figure 5.1 Autocorrelation of shear over depth interval 29-32 m. The solid curve is the autocorrelation of $\Delta u/\Delta z$, and the dashed curve is for $\Delta v/\Delta z$.

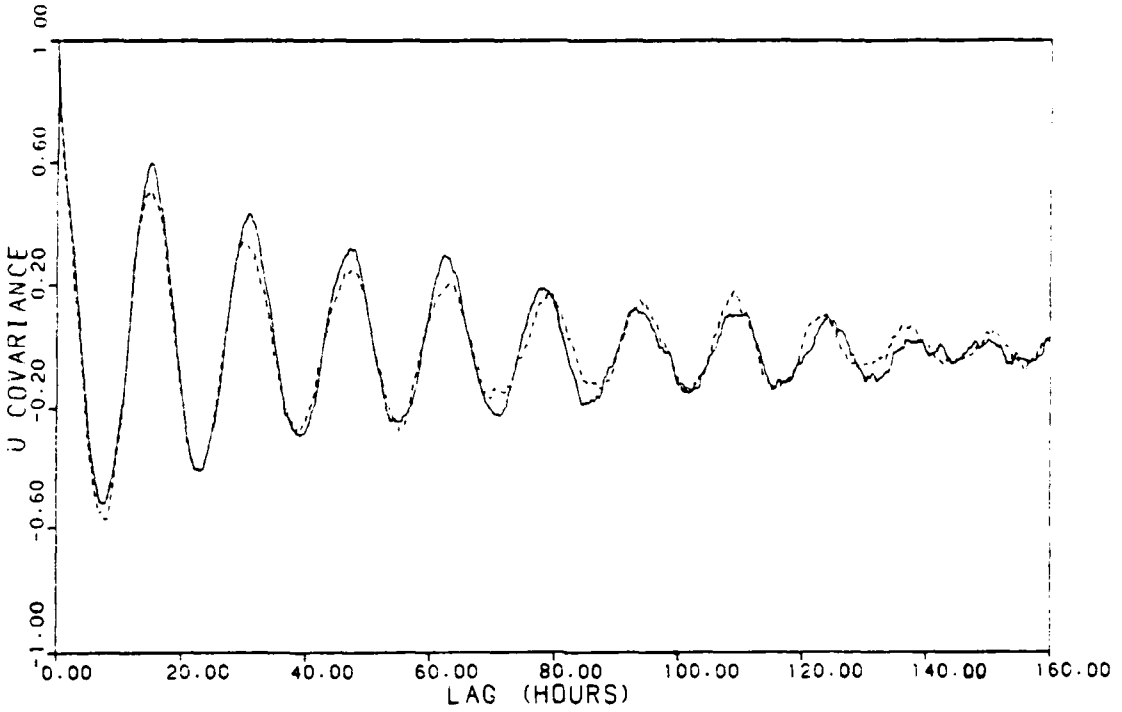


Figure 5.2 Autocorrelation of shear over depth interval 41-44 m. The solid curve is the autocorrelation of $\Delta u/\Delta z$, and the dashed curve is for $\Delta v/\Delta z$.

level. At this level, sample populations of a truly random parent population should fail the run test less than 20% of the time. (A detailed description of the run test may be found in Conover, 1971.) We find that the minimum subsampling interval is four hours.

This means that if we subsample at the rate of once per four hours, adjacent pairs of observations are nearly equally likely to be of the opposite and of the same signs. This result is in agreement with the autocorrelation function, which first passes through zero at 4 hours. We choose to use this definition of randomness, or "statistical independence." In all of the statistical tests in the remainder of Section 5, we subsample at 4 hour intervals. If the inertial amplitude remains correlated over a significantly longer interval, then all of the samples will not be statistically independent, and the number of independent samples will be overestimated. As a result, the tendency will be for a true null hypothesis to be rejected.

### 5.1.2 Smirnov Test for Identical Distributions

Before proceeding with the tests for Gaussianity, we first determine whether or not the distribution functions associated with the two populations of $\Delta u/\Delta z$ and $\Delta v/\Delta z$ observations are identical. For this purpose we use the two-sided Smirnov test described by Conover (1971). The test statistic T is defined to be

$$T = \sup_x \left| S_1(x) - S_2(x) \right| , \qquad (5.1)$$

where $S_1(x)$ and $S_2(x)$ are the observed distribution functions of $\Delta u/\Delta z$ and $\Delta v/\Delta z$, respectively. The symbol $\sup_x$

denotes supremum, or maximum value over the range of x. In other words, the test statistic is the greatest vertical distance between the distribution functions $S_1(x)$ and $S_2(x)$.

We analyzed all of the shear distributions in the upper thermocline, $\Delta u/\Delta z$ and $\Delta v/\Delta z$, for $\Delta z$ = 3, 6, 12, and 21 m. We first subsampled at 4 hour intervals, and then subtracted the means computed over the entire 19 day duration of the time series. The two resulting time series, each approximately of length 19x24/4 = 114 points, were sorted and the distribution functions computed. The Smirnov test is applicable even if the two sample populations are not equal in size (but in our case the populations were equal in size).

In all of the cases we studied, the null hypothesis--that the two distributions were identical--was accepted at the $\alpha$ = 0.20 level of significance. This result is not very surprising in light of Figures 4.2-4.5. In this set of figures, the individual components of mean-square shear, i.e., the variances of $\Delta u/\Delta z$ and $\Delta v/\Delta z$, are nearly equal. Therefore we do not expect significant differences between the statistical tests for $\Delta u/\Delta z$ and $\Delta v/\Delta z$ in Sections 5.2-5.4.

## 5.2 LILLIEFORS TEST FOR GAUSSIANITY

In this section we apply the Lilliefors test for Gaussianity (normality) to the horizontal components of vertical shear, $\Delta u/\Delta z$ and $\Delta v/\Delta z$. The null hypothesis is that the random sample has a Gaussian distribution, with unspecified mean and variance. In order to assure randomness, we subsample the shear components at 4 hour intervals, as discussed in Section 5.1.1.

Let $x_i$, $i = 1,2,...n$ be the measured samples of shear, $\Delta u/\Delta z$ or $\Delta v/\Delta z$. We normalize the sample values by subtracting out the mean $\bar{x}$ and dividing by the standard deviation $\sigma$;

$$z_i = \frac{x_i - \bar{x}}{\sigma} ; \tag{5.2}$$

$$\bar{x} = \frac{1}{n} \sum_{i=1}^{n} x_i ; \tag{5.3}$$

$$\sigma = \left[ \frac{1}{n-1} \sum_{i=1}^{n} (x_i - \bar{x})^2 \right]^{1/2} . \tag{5.4}$$

The new samples $z_i$, $i=1,2,...,n$ have zero mean and unity standard deviation. The "standard" ($\bar{z}=0$, $\sigma_z=1$) Gaussian probability density function is

$$f(z) = (2\pi)^{-1/2} \exp(-z^2/2) , \tag{5.5}$$

and the associated "standard" distribution function is

$$F(z) = \int_{-\infty}^{z} f(z)\, dz = \frac{1}{2} + \mathrm{erf}(z) , \tag{5.6}$$

where erf is the error function.

Figure 5.3 is a representative histogram, showing the observed probability density of $\Delta u/\Delta z$ computed from the current meter pair at depths 41-44 m. The abscissa has been normalized as in equations (5.2)-(5.4). The observed probability density is compared with the Gaussian function (5.5), denoted by X's. The agreement is appealing to the eye, but we need an objective test of the goodness of fit.

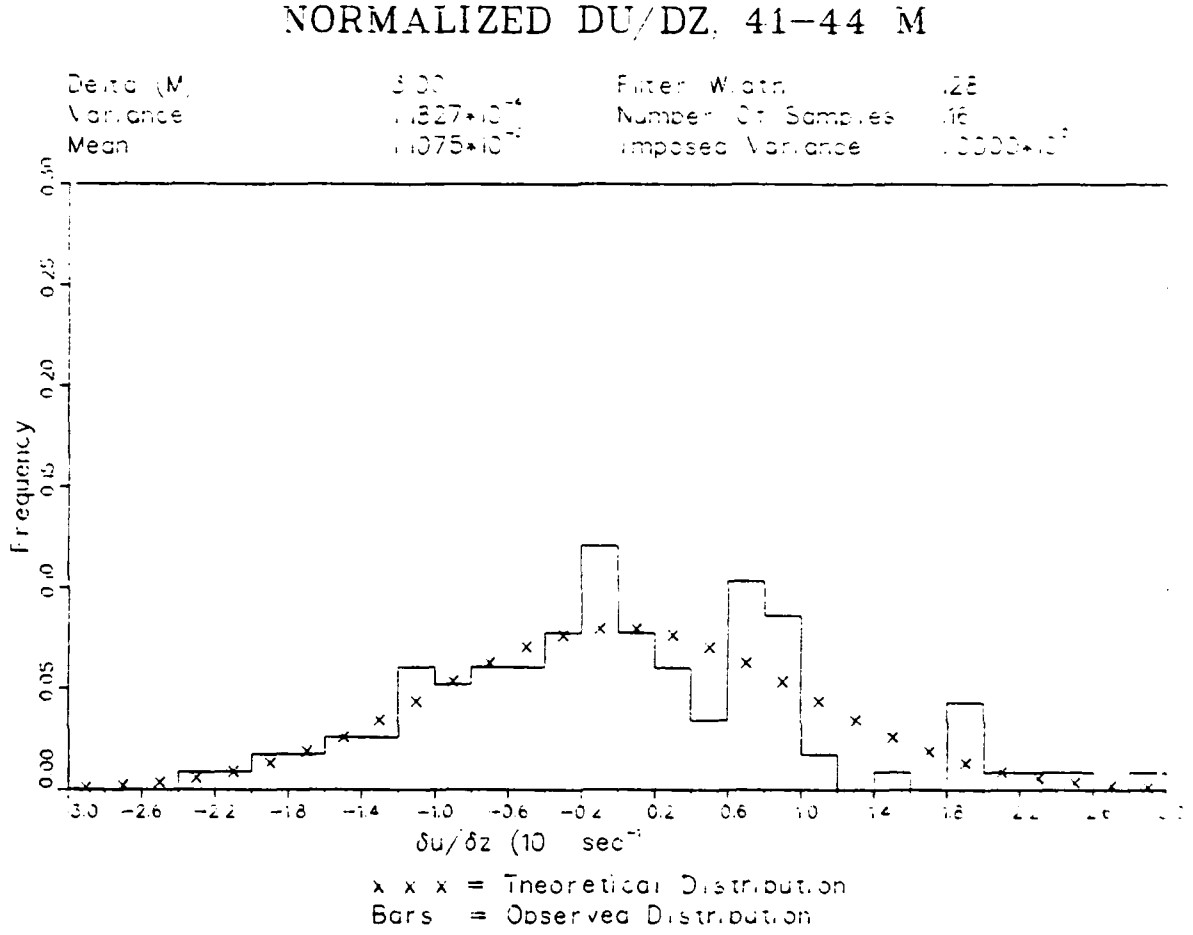


• Figure 5.3 Frequency distribution histogram of shear component du/dz over 41-44 m. The 19-day record has been subsampled at 4 hour intervals, and normalized by the standard deviation. The crosses denote a normalized Gaussian function, from equation (5.5).

Some authors use the chi-square test for goodness of fit, but the results depend somewhat on the number of bins chosen for the test. Instead, we prefer to use a test of the "Kolmogorov-Smirnov type", that is, one based on the distribution function. The Lilliefors test for Gaussianity is of this type.

Figure 5.4 is the observed probability distribution of $\Delta u/\Delta z$, corresponding to the same probability density histogram shown in Figure 5.3. The dashed curve is the standard function distribution (5.6). The Lilliefors test statistic T is computed from the standard distribution function F(z) in (5.6), and from the observed distribution S(z) of the normalized shear z;

$$T = \sup_z |F(z) - S(z)| \quad . \tag{5.7}$$

Thus, T is the maximum vertical distance between the standard distribution function (dashed curve) and the observed distribution (solid curve) in Figure 5.4. We can estimate the test statistic T graphically. We find that for this case, T = 0.049, which occurs at z = 1.0. This distance falls well within the 80% confidence interval 0.068. Therefore the null hypothesis (that the distribution is Gaussian) is accepted at the $\alpha = 0.20$ level of significance. Conover (1971) says that acceptance of the null hypothesis does not necessarily mean that the parent population is Gaussian. But it does mean that the Gaussian distribution is not an unreasonable approximation to the true unknown distribution.

Since we need to analyze a large number of cases, in practice we do not evaluate T graphically, but we program a computer code to calculate it. Table 5.1 lists the critical levels of significance $\hat{\alpha}$ for all of the seasonal

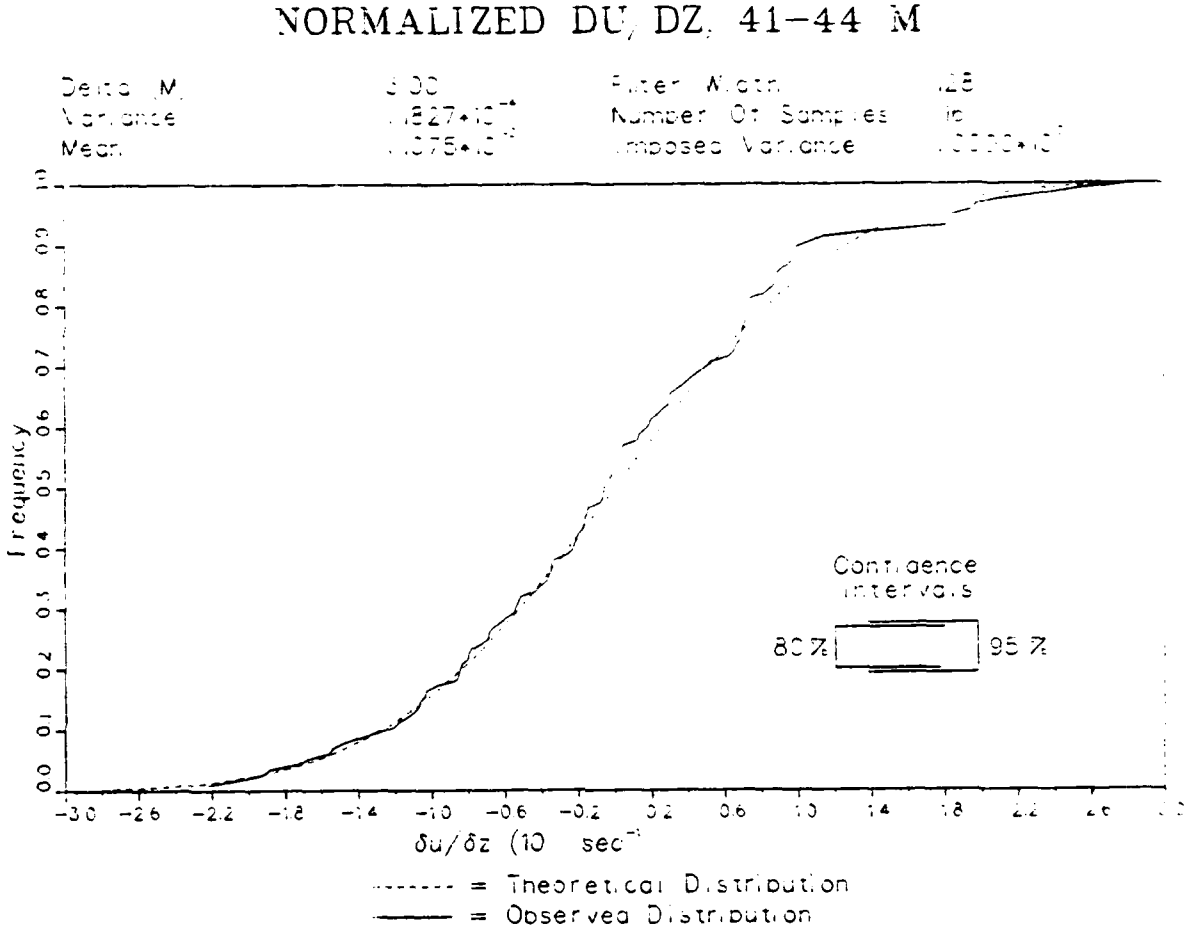


Figure 5.4 Cumulative distribution of shear component du/dz over 41-44 m. The 19-day record has been sub-sampled at 4 hour intervals, and normalized by the standard deviation. The dashed line is the error function cumulative distribution, from equation (5.6). The Lilliefors test statistic, defined as the maximum vertical distance between the two distribution curves, is 0.047. This value falls well within the 80% confidence interval.

thermocline shear distributions in the depth range 26-92 m. The critical level $\hat{\alpha}$ is defined (Conover, 1971) as the smallest significance level at which the null hypothesis would be rejected for the given observation. The results show that the Gaussian distribution is a reasonable approximation to the true distribution. About 85% of the 48 cases were accepted by the Lilliefors test at the 0.20 level of significance.

Table 5.1

Lilliefors Gaussianity Test Results

Distribution of critical levels $\hat{\alpha}$ for $\Delta u/\Delta z$ and $\Delta v/\Delta z$ for 3, 6, 12, and 21 m separations.

| $\Delta z$ = | 3 m | 6 m | 12 m | 21 m | TOTAL |
|---|---|---|---|---|---|
| $\hat{\alpha} < 0.01$ | 2 | 0 | 0 | 0 | 2 |
| $0.05 > \hat{\alpha} \geq 0.01$ | 0 | 2 | 1 | 0 | 3 |
| $0.10 > \hat{\alpha} \geq 0.05$ | 0 | 1 | 0 | 0 | 1 |
| $0.20 > \hat{\alpha} \geq 0.10$ | 0 | 0 | 0 | 1 | 1 |
| $\hat{\alpha} \geq 0.20$ | 14 | 11 | 9 | 7 | 41 |
| TOTAL | 16 | 14 | 10 | 8 | 48 |

## 5.3 STATISTICAL MODEL APPLICATION: THE KOLMOGOROV TEST

In Section 5.2 we applied the Lilliefors test to our shear data, and showed that $\Delta u/\Delta z$ and $\Delta v/\Delta z$ are well described by Gaussian distributions. The mean and variance were not previously specified, but instead were estimated from the data.

In this section we apply the statistical model developed in Section 4 to estimate the variance of $\Delta u/\Delta z$ and $\Delta v/\Delta z$. The variance is estimated from the least-squares fit in Figure 4.6, according to the formula

$$\sigma^2 \equiv \frac{1}{2}\overline{S^2} \approx \overline{N^2}\,\frac{1.85\Delta z - 2.8}{\Delta z^2} \qquad (5.8)$$

As we are only interested in near-inertial frequency fluctuations, and not in long-term trends, we have subtracted the mean from each shear record.

We applied the Kolmogorov goodness-of-fit test to each of the shear records in the seasonal thermocline in the depth range 26-70 m. The shear records over 70-92 m were not included in this test, because the salinity gradient's contribution to $N^2$ in this interval is of comparable importance to that of the temperature gradient. The test statistic is computed in the same way as for the Lilliefors test, eq. (5.7). The difference is that the variance is estimated by (5.8), and the critical level values are evaluated from a different set of tables.

Table 5.2 lists the distribution of critical levels of significance $\hat{\alpha}$ for all the seasonal thermocline shear records. In 43 out of 46, or 93% of all cases, the null hypothesis that the shear distribution is Gaussian with the variance given by (5.8), is accepted at the 0.20 level of significance.

Table 5.2

Kolmogorov Goodness-of-Fit Test Results

Distribution of critical levels $\hat{\alpha}$ for $\Delta u/\Delta z$ and $\Delta v/\Delta z$ for 3, 6, 12, and 21 m separations.

| $\Delta z$ = | 3 m | 6 m | 12 m | 21 m | TOTAL |
|---|---|---|---|---|---|
| $\hat{\alpha} < 0.01$ | 0 | 0 | 0 | 0 | 0 |
| $0.05 > \hat{\alpha} \geq 0.01$ | 0 | 0 | 0 | 0 | 0 |
| $0.10 > \hat{\alpha} \geq 0.05$ | 1 | 1 | 0 | 0 | 2 |
| $0.20 > \hat{\alpha} \geq 0.10$ | 1 | 0 | 0 | 0 | 1 |
| $\hat{\alpha} \geq 0.20$ | 14 | 13 | 10 | 6 | 43 |
| TOTAL | 16 | 14 | 10 | 6 | 46 |

## Section 6
## INSTANTANEOUS PREDICTIONS OF SHEAR

In this Section we address the following question:

> If we have a 15-minute-average observation of local density stratification, with what degree of certitude can we predict the value of shear?

We have already shown, in Section 5, that $\overline{S^2}$ and $\overline{N^2}$ are well correlated, statistically, over long time scales. Over a long period however, $N^2$ can change significantly. Therefore we ask if it is possible to predict $S^2$ (over some vertical separation $\Delta z$) from a short-period average $N^2$, say, as short as 15 minutes.

Figure 6.1 shows a time series of 15-minute samples of $N^2$ and $S^2$, for three days, measured between depths 29 and 32 m. We see that $N^2$ and $S^2$ are often well correlated, even over short time scales.

This high degree of correlation can be understood, at least in part, in terms of episodes of shear instability. From measurements of shear and stratification over a 7 m vertical separation using the microscale sensing array, Eriksen (1978) argues that the flow is dynamically limited by shear stability. He shows that the distribution of Richardson number $Ri = N^2/S^2$ falls off sharply below $Ri = 0.25$. This cutoff is evocative of theoretical predictions of shear instability. A likely candidate mechanism is the Kelvin-Helmholtz instability, first observed by Woods (1968) in the seasonal thermocline. The theoretical

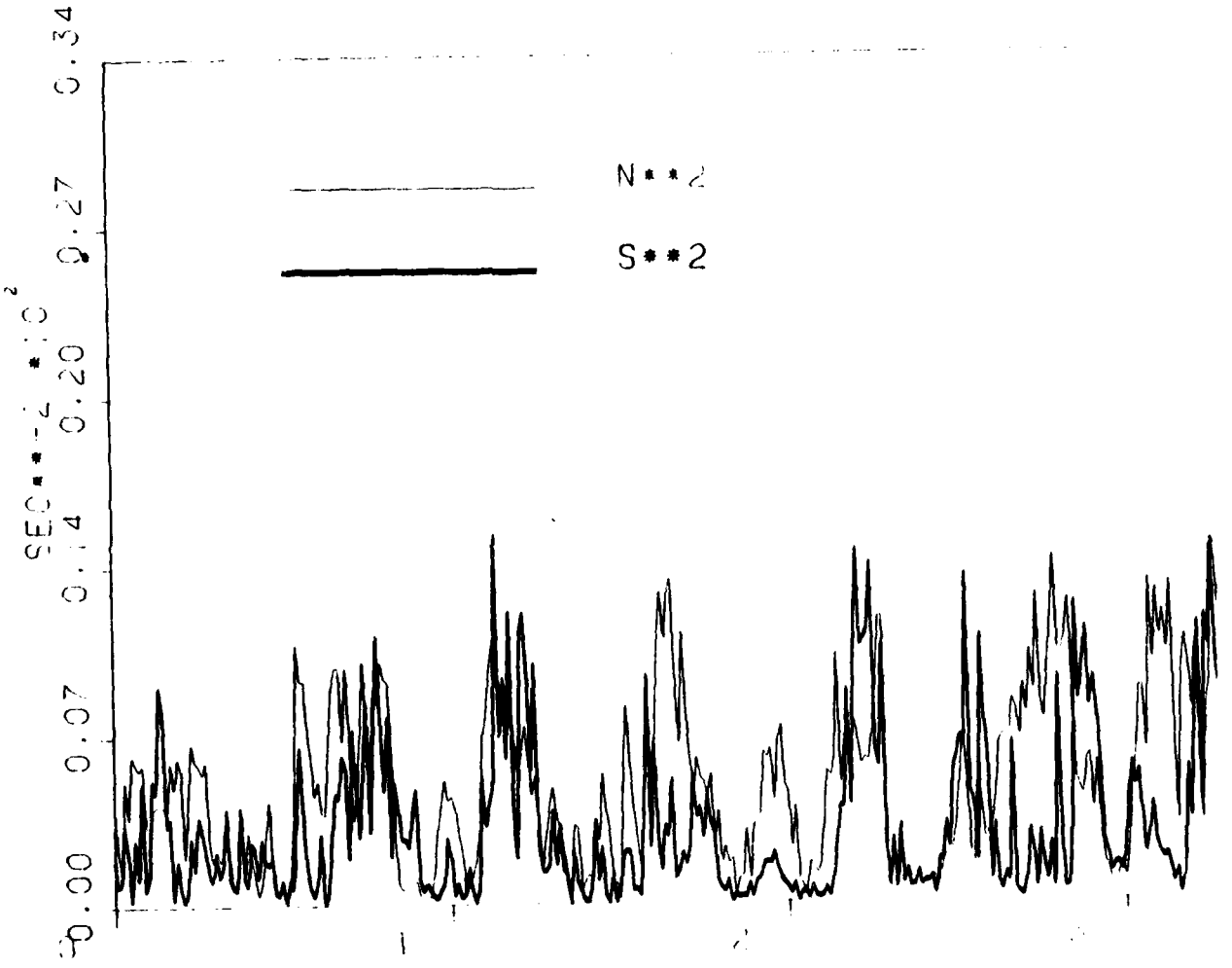


Figure 6.1 Time series of 15-minute averaged samples of $N^2$ and $S^2$, for 3½ days, measured between depths 29 and 32 m.

stability analysis by Miles and Howard (1964) shows that the most unstable disturbance has a wavelength

$$\lambda = 7.5\ h, \tag{6.1}$$

where h is the thickness of a shear layer. Woods (1968) observed a sheet and layer structure in the temperature and velocity profiles. He found that in the vast majority of cases, the layer thickness h fell in the range $8<h<15$ cm, and that in all measured cases, the relationship between $\lambda$ and h fell within 20% of equation (6.1). Thus it seems plausible that shear instability may be occurring over a small vertical scale.

Other mixing mechanisms, such as the convective instability proposed by Orlanski and Bryan (1969), may also be contributing to the correlation between $N^2$ and $S^2$. This remains a speculative area; more observational and theoretical work is needed.

For now though, we seek only to quantify the correlation between $N^2$ and $S^2$ over a 15 minute time scale. We quantified the correlation in two ways. First, we computed the linear correlation coefficient between $N^2$ and $S^2$ for all pairs of current meters in the seasonal thermocline, over the depth range between 26 and 70 m, using separations of 3, 6, 12 and 21 m. Table 6.1 shows the upper and lower limits of the correlation coefficient for each vertical separation. For the most part, the correlation coefficients fall in the range from 0.30 to 0.54. Values greater than 0.20 are correlated at the 5% level of significance. Therefore we can say that for most of the data records, the $N^2$-$S^2$ correlation is statistically significant.

Table 6.1

LOWER AND UPPER LIMITS OF LINEAR CORRELATION COEFFICIENTS BETWEEN 15-MINUTE AVERAGED OBSERVATIONS OF $N^2$ AND $S^2$

| | Correlation | |
|---|---|---|
| $\Delta z$ | Lower Limit | Upper Limit |
| 3 m | .34 | .54 |
| 6 m | .40 | .53 |
| 12 m | .30 | .52 |
| 21 m | .15 | .46 |

The second way in which we quantified the correlation was by means of the distribution of $S^2/N^2$ measurements. Figure 6.2 shows a histogram of samples of $S^2/N^2$ measurements over the depth interval 41-44 m, and Figure 6.3 shows the corresponding cumulative distribution function. From Table 4.2, the expected value of $\overline{S^2}/\overline{N^2}$ over a 3 m interval is 0.61. We can use Figure 6.3 to show that an estimate of $S^2 = 0.61N^2$ is accurate within a factor of two, 47% of the time, and within a factor of four, 74% of the time.

Table 6.2 summarizes the results for all pairs of current meters in the seasonal thermocline, between depths 26 and 70 m, separated by 3, 6, 12 and 21 m. As $\Delta z$ increases, the accuracy with which we can predict $S^2$ also increases. The reason for this trend is that the temporal fluctuations of $N^2$ and $S^2$ tend toward smaller values relative to $\overline{N^2}$ and $\overline{S^2}$, as $\Delta z$ increases.

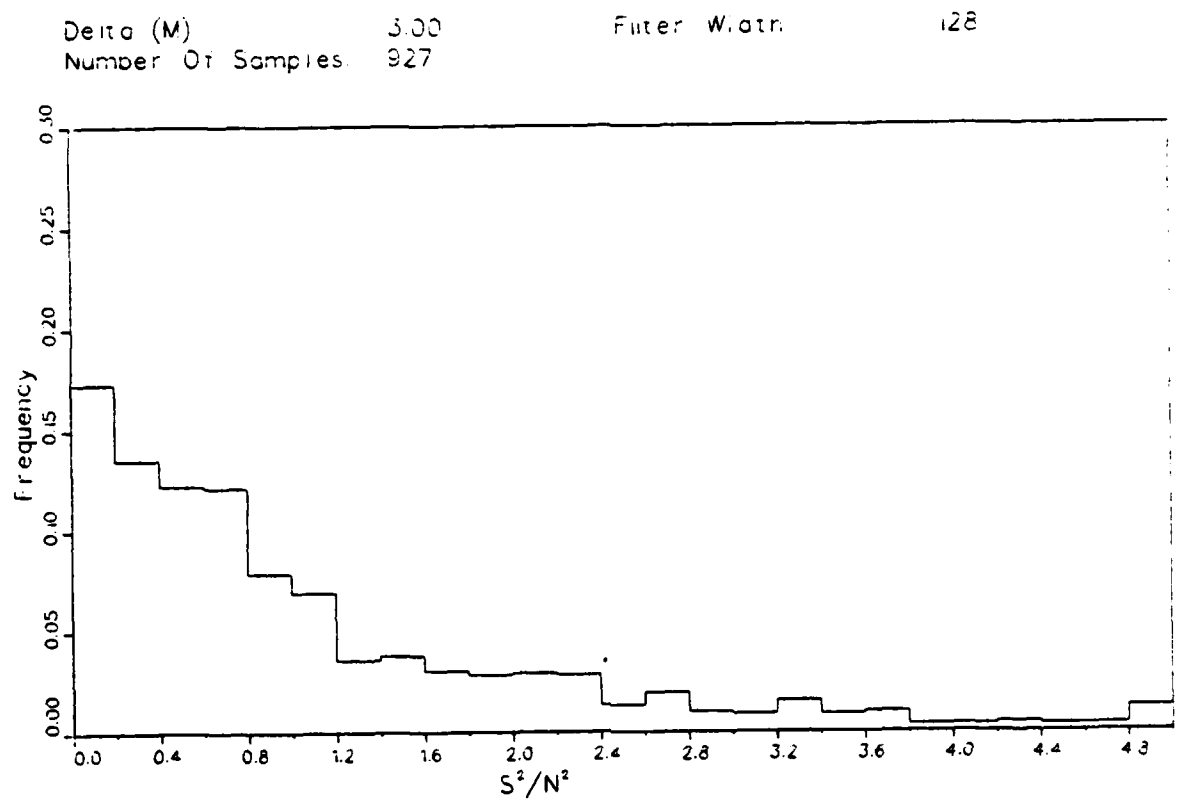


Figure 6.2 Probability density histogram of $S^2/N^2$ over the depth interval 41-44 m. Each sample is the ratio of 15-minute averages of $S^2$ and $N^2$. See also Figure 6.3.

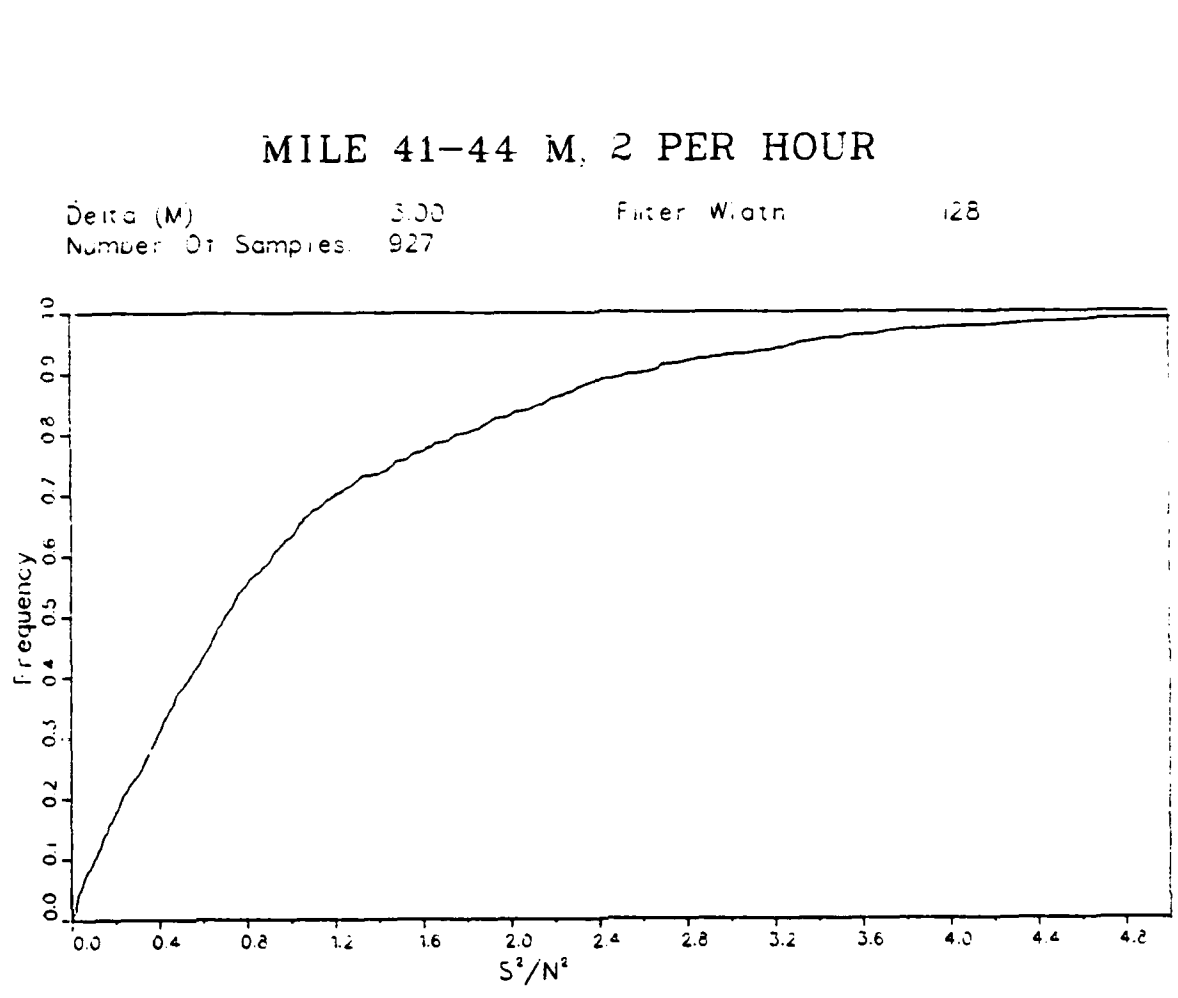


Figure 6.3 Cumulative distribution function of $S^2/N^2$ over the depth interval 41-44 m. Each sample is the ratio of 15-minute averages of $S^2$ and $N^2$.

Table 6.2

AVERAGE PERCENTAGE OF 15-MINUTE $N^2$ OBSERVATIONS FROM WHICH WE CAN PREDICT $S^2$ WITHIN A FACTOR OF 2 AND 4

| | Accuracy Factor | |
|---|---|---|
| $\Delta z$ | 2 | 4 |
| 3 m | 45% | 76% |
| 6 m | 51% | 79% |
| 12 m | 54% | 79% |
| 21 m | 60% | 85% |

## Section 7
## SUMMARY AND RECOMMENDATIONS

Our most important result is the validation of a statistical model of mean-square shear $\overline{S^2}$, first proposed by Grabowski (1981). The model is derived from an idealized version of the vertical wavenumber shear spectrum of Gargett et al. (1981). This composite spectrum was assimilated from vertical profiles of shear in the main thermocline. The model predicts that $\overline{S^2}$ is proportional to $\overline{N^2}/\Delta z$, where $\Delta z$ is the vertical separation over which shear is measured. We compare the model's predictions for mean-square velocity differences with differences calculated from various pairs of MILE current meters, and find qualitative agreement.

In general, $\overline{S^2}$ is proportional to $\overline{N^2}$, but in the seasonal thermocline, both quantities vary rapidly with depth. Therefore, vertical shear profilers cannot measure statistically reliable spectra in the seasonal thermocline. However, our statistical model allows us to relate shear spectra obtained from deep vertical profiles to current meter-derived $\overline{S^2}$, as a function of $\overline{N^2}$ and $\Delta z$. Thus we can extend the range of validity of the Gargett et al. (1981) composite spectrum into the seasonal thermocline.

Inertial oscillations tend to dominate the higher-frequency fluctuations of the shear vector. Therefore, over the course of an inertial period, the probability distributions of $\Delta u/\Delta z$ and $\Delta v/\Delta z$ frequently are bimodal. Over the course of several inertial oscillations, slow variations in the inertial amplitude tend to smear out the probability distributions, and they approach Gaussianity.

We have shown that mean square shear is nearly isotropic. Figures 4.2-4.6 show that $\overline{(\Delta u/\Delta z)^2} \approx \overline{(\Delta v/\Delta z)^2} \approx \overline{S^2}/2$, where the overbars denote 19 day averages. We used our statistical model for $\overline{S^2}$ to parameterize the Gaussian distributions of the individual shear components. These parameterized distributions agree very well with the observed distributions.

Shear and stratification are significantly correlated over short time scales, as well. Fifteen-minute averaged samples of $N^2$ and $S^2$ measured over $\Delta z$=3 m have correlation coefficients in the range 0.34-0.54. We showed that knowing $N^2$ over a 3 m vertical interval allows us to estimate $S^2$ within a factor of two, 46% of the time, and within a factor of four, 75% of the time. Similar results were obtained over wider vertical intervals.

It is not clear from the MILE current meter records whether shear variability is primarily due to

- temporal variability,
- vertical variability due to vertical displacements of the current meters, or
- vertical variability due to vertical displacements of the shear field by internal waves and Ekman pumping,

or some combination of these factors. An analysis of shear observations in an isopycnal or isothermal (constant density or temperature) coordinate frame should significantly increase our understanding of shear variability. An analysis

of this type could be performed using existing data. For example, the MILE data set discussed in this report would be appropriate. Shear variability due to vertical displacements by internal waves and Ekman pumping could be largely filtered out, leaving a record whose variability is due to purely temporal effects. This technique would be ideal for studying the autocorrelation properties of shear, and the coherence between shear and wind stress.

## REFERENCES


Briscoe, M. G., 1977: Gaussianity of internal waves. J. Geophys. Res., **82**, 2117-2126.

Conover, W. J., 1971: Practical Nonparametric Statistics. John Wiley & Sons, New York, First Edition.

Davis, R. E., R. deSzoeke, D. Halpern, and P. Niiler, 1981: Variability in the upper ocean during MILE. Part I: The heat and momentum balances. Deep-Sea Res., **28**, 1427-1451.

Eriksen, C. C., 1978: Measurements and models of fine structure, internal gravity waves, and wave breaking in the deep ocean. J. Geophys. Res., **83**, 2989-3009.

Gargett, A. E., P. J. Hendricks, T. B. Sanford, T. R. Osborn, A. J. Williams III, 1981: A composite spectrum of vertical shear in the upper ocean. J. Phys. Oceanography, **11**, 1258-1271.

Grabowski, W., 1980: Modeling of internal-wave induced shear progress report. Ocean Physics Division, OPD TN-80-201-01, Science Applications, Inc., McLean, Virginia.

Grabowski, W., 1981: Spectral model predictions of mean-square distortion rates. Science Applications, Inc., Ocean Physics Division, OPD TN 81-201-01.

Halpern, D., R. A. Weller, M. G. Briscoe, R. E. Davis, and J. R. McCullough, 1981: Intercomparison tests of moored current measurements in the upper ocean. J. Geophys. Res., **86**, 419-428.

Hebenstreit, G. T. and W. Grabowski, 1981: Statistical modeling of shear in the upper ocean. SAI-82-382-WA, Ocean Physics Division, Science Applications, Inc., McLean, Virginia, 71 pp.

Kundu, P. K., 1976: An analysis of inertial oscillations observed near Oregon coast. J. Phys. Oceanography, **6**, 879-893.

Lambert, R. B., Jr. and S. L. Patterson, 1980: Review of upper ocean vertical shear. Ocean Physics Division Technical Report 80-201-02, Science Applications, Inc., McLean, Virginia, 170 pp. (CONFIDENTIAL)

Levine, M. D., 1981: Dynamic response of the VACM temperature sensor. Deep-Sea Res., **28**, 1401-1408.

McCullough, J. R., 1975: Vector-averaging current meter speed calibration and recording technique. Tech. Report 75-44, Woods Hole Oceanographic Institution, Woods Hole, Massachusetts.

Mamayev, O. I., 1975: Temperature-Salinity Analysis of World Ocean Waters. American Elsevier Publishing Company, Inc., New York.

Miles, J. W., and L. N. Howard, 1964: Note on a heterogeneous shear flow. J. Fluid Mech., **20**, 331-336.

Orlanski, I., and K. Bryan, 1969: Formation of the thermocline step structure by large-amplitude internal gravity waves. J. Geophys. Res., **74**, 6975-6983.

Patterson, S. L., F. C. Newman, D. M. Rubenstein, and R. B. Lambert, Jr., 1981: Spatial distribution of vertical shear. SAI-82-294-WA, OPD-TR-81-201-02, Ocean Physics Division, Science Applications, Inc., McLean, Virginia, 137 pp.

Perkins, H., 1970: Inertial oscillations in the Mediterranean. Ph.D. thesis, MIT-Woods Hole, 155 pp.

Rabiner, L. R., and B. Gold, 1975: Theory and Application of Digital Signal Processing. Prentice-Hall, Inc., Englewood Cliffs, New Jersey.

Rubenstein, D. M., 1981: Models of near inertial vertical shear. Science Applications, Inc., Ocean Physics Division, SAI-82-546-WA, OPD-81-274-04, 62 pp.

Simpson, J. H., 1975: Observations of small scale vertical shear in the ocean. Deep-sea Res., **22**, 619-627.

Woods, J. D., 1968: Wave-induced shear instability in the summer thermocline. J. Fluid Mech., **32**, 791-800.


DATE
ILME

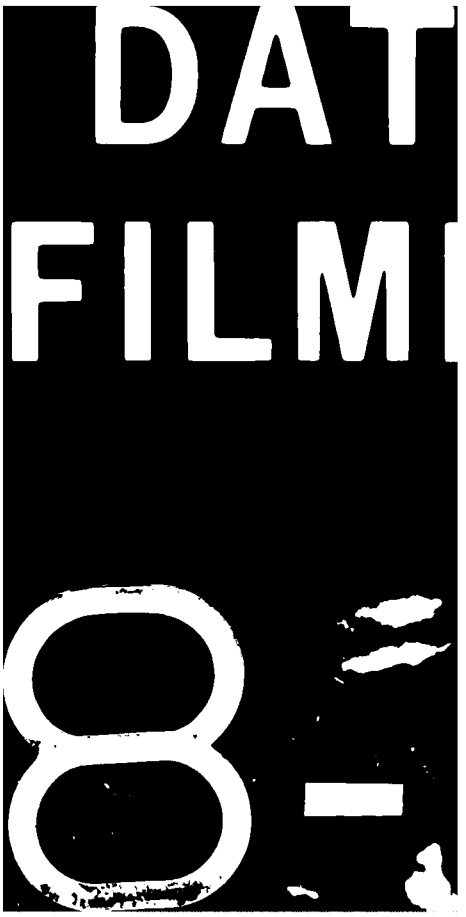
DAT
FILM
8-